Supplementary Information

Interface Formation between CdS and Alkali Post-Deposition Treated $Cu(In,Ga)Se_2$ Thin Film Solar Cell Absorbers – Key to Understanding the Efficiency Gain?

Penghui Yang,[†] *Regan G. Wilks,*[†,‡] *Wanli Yang,*[§] *and Marcus Bär*[*,†,‡,∥,#]

[†]Department. Interface Design, Helmholtz-Zentrum Berlin für Materialien und Energie GmbH, 12489 Berlin, Germany.

[‡]Energy Materials In-Situ Laboratory Berlin (EMIL), Helmholtz-Zentrum Berlin für Materialien und Energie GmbH, 12489 Berlin, Germany.

[§]Advanced Light Source Lawrence Berkeley National Laboratory, Berkeley, California 94720, USA

[∥]Department of Chemistry and Pharmacy, Friedrich-Alexander-Universität Erlangen-Nürnberg, Egerlandstr. 3, 91058 Erlangen, Germany

[#]Helmholtz Institute Erlangen-Nürnberg für Renewable Energy (HI-ERN), Albert-Einstein-Str. 15, 12489 Berlin, Germany

Corresponding Author

*E-mail: marcus.baer@helmholtz-berlin.de.

1. Basic principles of the used characterization techniques

When an x-ray photon impinges on a material surface, it interacts with the sample. In general, this causes electrons to be excited from an occupied to an unoccupied electronic state or (if the excitation energy is sufficient, i.e. > than the electron binding energy + the work function of the sample) to leave the sample. The remaining kinetic energy of these photoelectrons is then measured by, e.g. an electron analyzer. Since the electron's binding energy (and thus the measured kinetic energy) is element specific, the chemical composition of the sample can be probed that way. Due to the short inelastic mean free path (IMFP) of electrons at kinetic energies attainable with soft x-ray excitation, laboratory-based x-ray photoelectron spectroscopy measurements (XPS, generally using Mg K_α or Al K_α excitation) give a surface-sensitive view of the elements present in the sample. Since the intensity of the XPS line is directly related to the amount of the element present in the sample, the (surface) composition of the studied sample can (under certain assumptions, see e.g. Ref.[1] for more details) be derived. Furthermore, since the binding energy of a core electron of an element is influenced by the chemical bonding of that element (due to e.g. changes in electrostatic shielding upon bond formation – induced changes in the valence electron density of states), careful analysis of energy position and spectral shape of the measured XPS lines will also give insights into the chemical environment of the probed element.

In the x-ray emission process, the core hole created upon x-ray irradiation induced electron excitation (see above) is filled by a lower binding-energy electron, causing the emission of a photon. In x-ray emission spectroscopy (XES), the thus emitted photons are probed by a wavelength-dispersive x-ray spectrometer. Since XES is element-specific, it is an excellent tool to probe the local chemical structure. The probability for this process is very small; therefore, the experiment has to be performed at high-brightness synchrotron radiation sources. Since XES is a photon-in – photon-out process, its information depth is governed by the x-ray

attenuation length in the probed material and thus approximately 1 – 2 orders of magnitude larger than that of XPS (for more details see Ref.[2]).

2. Survey and detail spectra: Quantification

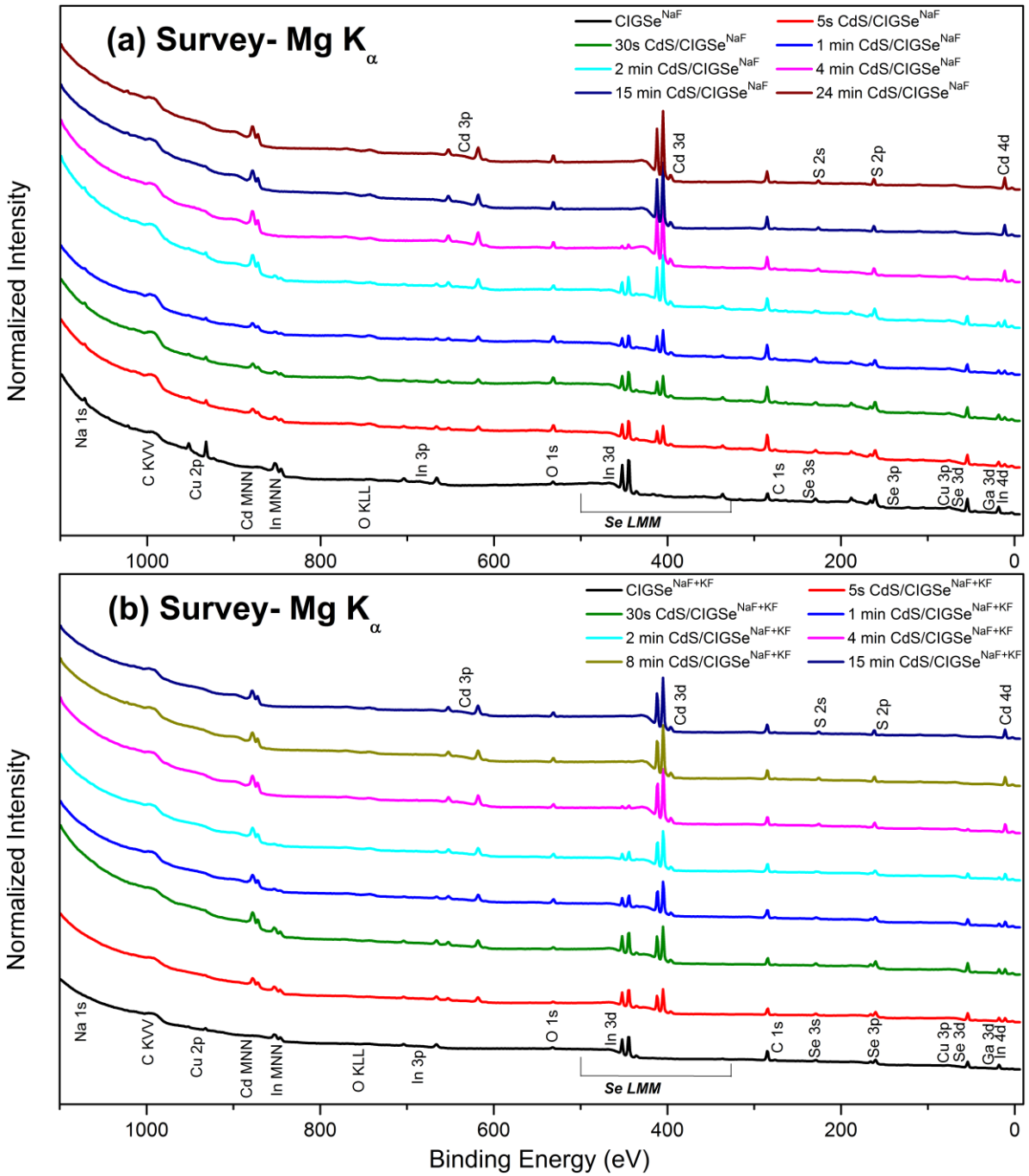

Figure S1. XPS survey spectra (normalized to background at a binding energy of 0 eV) of CdS/CIGSe^{NaF} (a) and CdS/CIGSe^{NaF+KF} (b) with increasing CBD time (varied between 0 and 24 [15] min). All the spectra were measured with excitation energies of hν=1253.56 eV (Mg K_α). All prominent photoemission and Auger lines are labeled. Spectra are vertically offset for clarity.

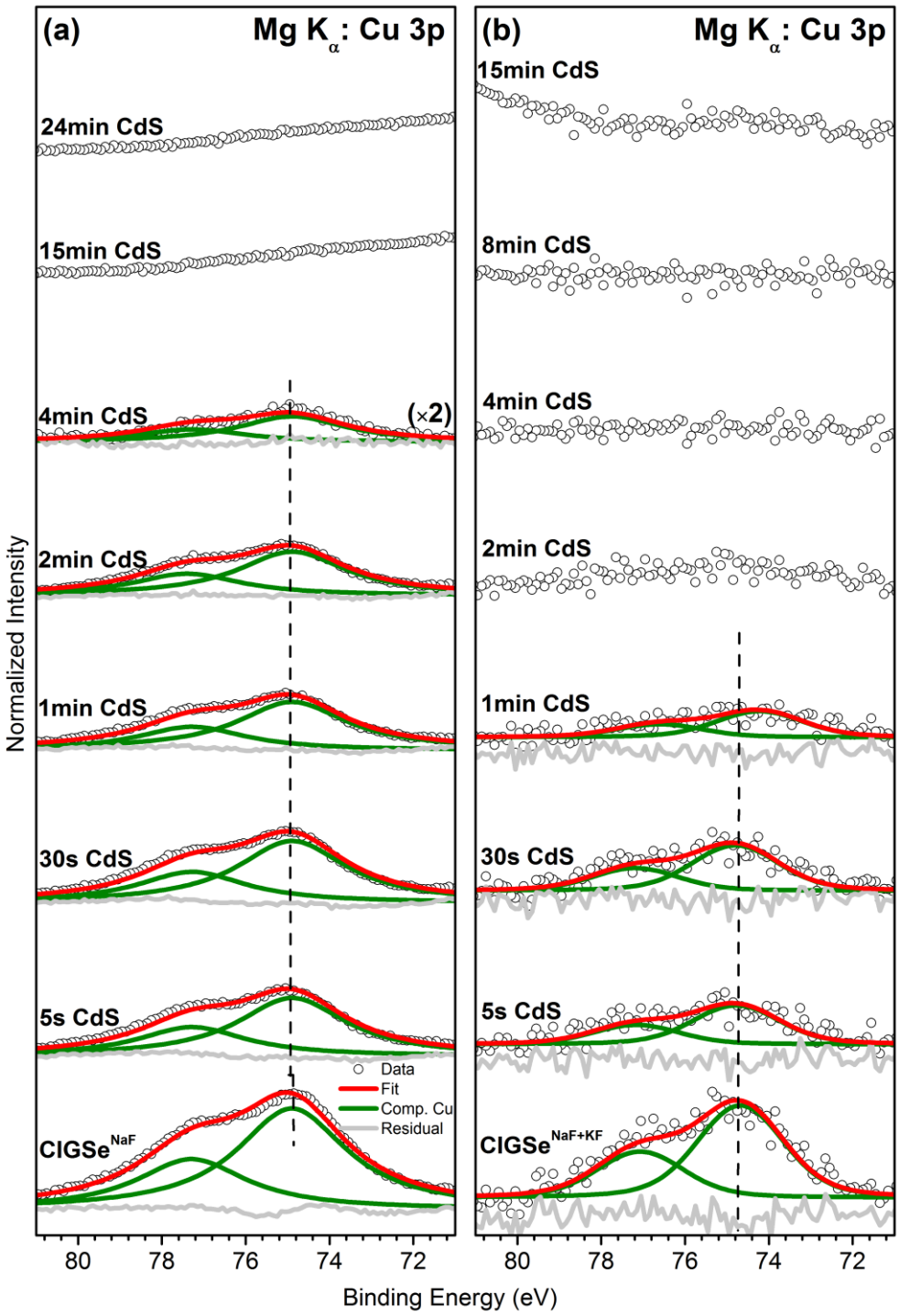

Figure S2. Cu 3p XPS data with respective Voigt fits of the CdS/CIGSe^{NaF} (a) and CdS/CIGSe^{NaF+KF} (b) sample series, measured with excitation energies of 1253.56 eV (Mg K_α). All spectra are displayed after subtraction of a linear background. For each fit, the residual is shown as well. Note the different magnification factors. Spectra are vertically offset for clarity.

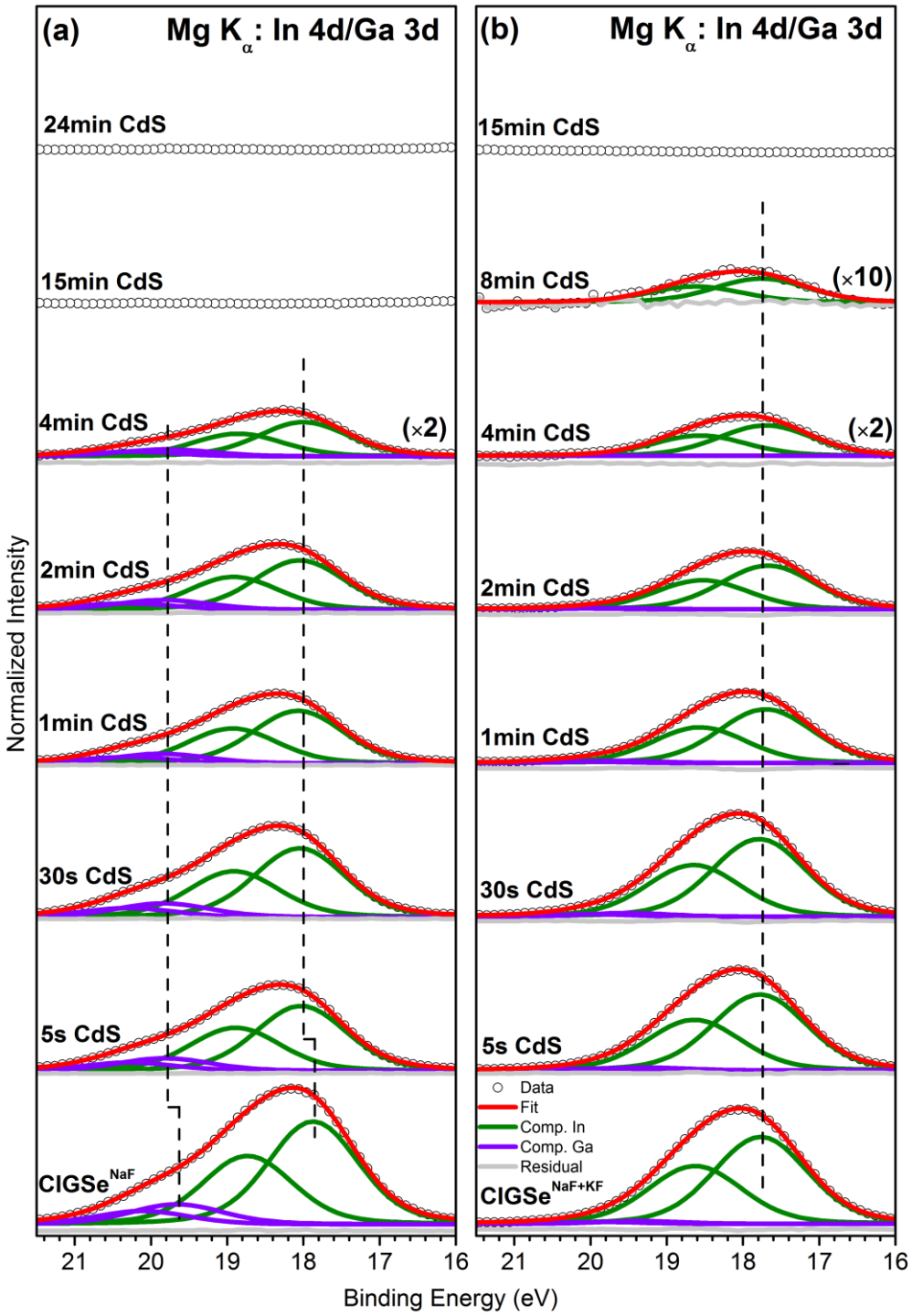

Figure S3. In 4d/Ga 3d XPS data with respective Voigt fits of the CdS/CIGSe^{NaF} (a) and CdS/CIGSe^{NaF+KF} (b) sample series, measured with excitation energies of 1253.56 eV (Mg K_α). All spectra are displayed after subtraction of a linear background. For each fit, the residual is shown as well. Note the different magnification factors. Spectra are vertically offset for clarity.

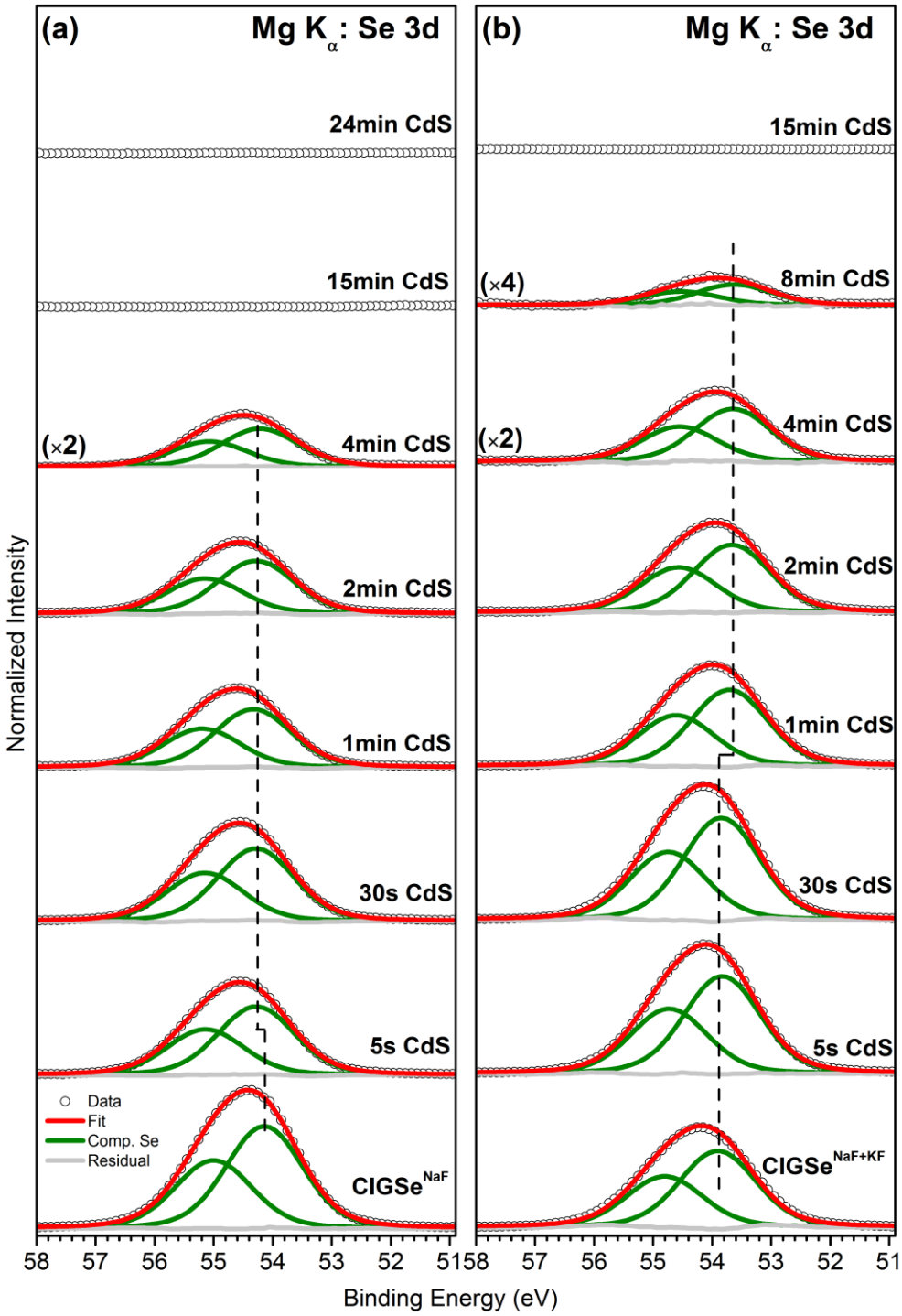

Figure S4. Se 3d XPS data with respective Voigt fits of the CdS/CIGSe^{NaF} (a) and CdS/CIGSe^{NaF+KF} (b) sample series, measured with excitation energies of 1253.56 eV (Mg K_α). All spectra are displayed after subtraction of a linear background. For each fit, the residual is shown as well. Note the different magnification factors. Spectra are vertically offset for clarity.

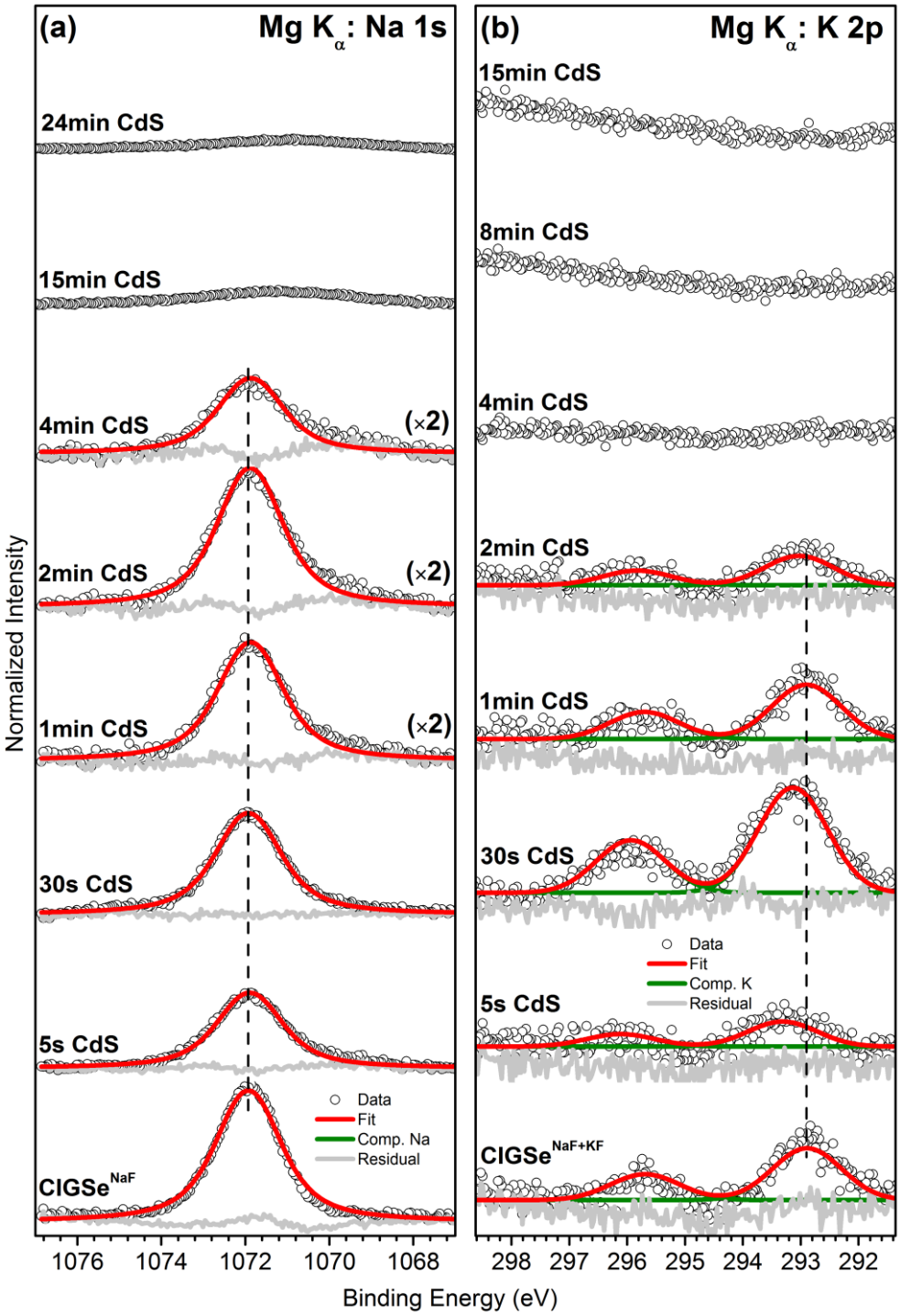

Figure S5. Na 1s (a) and K 2p (b) XPS data with respective Voigt fits of the CdS/CIGSe^{NaF} (a) and CdS/CIGSe^{NaF+KF} (b) sample series, measured with excitation energies of 1253.56 eV (Mg K_α). All spectra are displayed after subtraction of a linear background. For each fit, the residual is shown as well. Note the different magnification factors. Spectra are vertically offset for clarity.

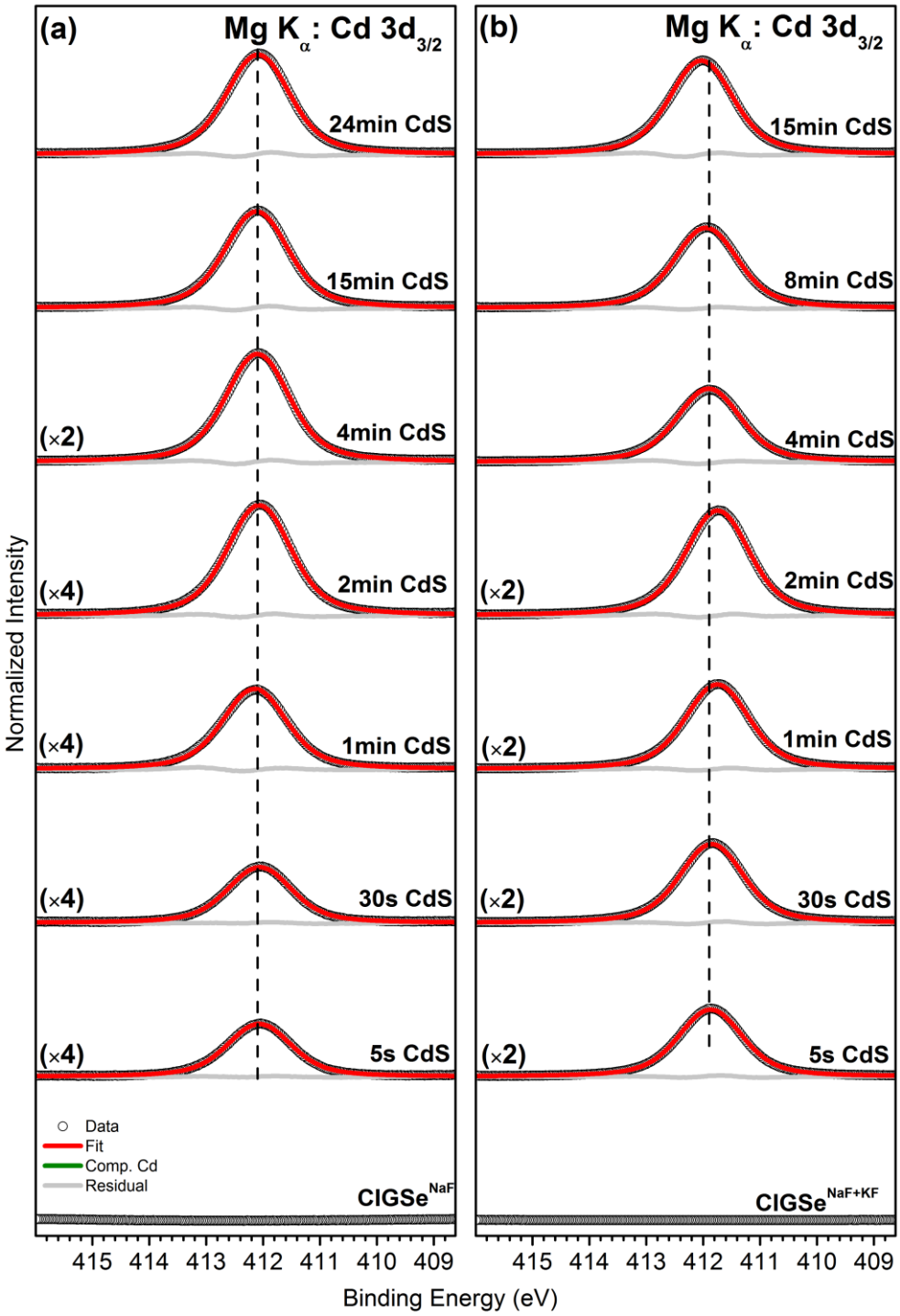

Figure S6. Cd 3d XPS data with respective Voigt fits of the CdS/CIGSe^{NaF} (a) and CdS/CIGSe^{NaF+KF} (b) sample series, measured with excitation energies of 1253.56 eV (Mg K_α). All spectra are displayed after subtraction of a linear background. For each fit, the residual is shown as well. Note the different magnification factors. Spectra are vertically offset for clarity.

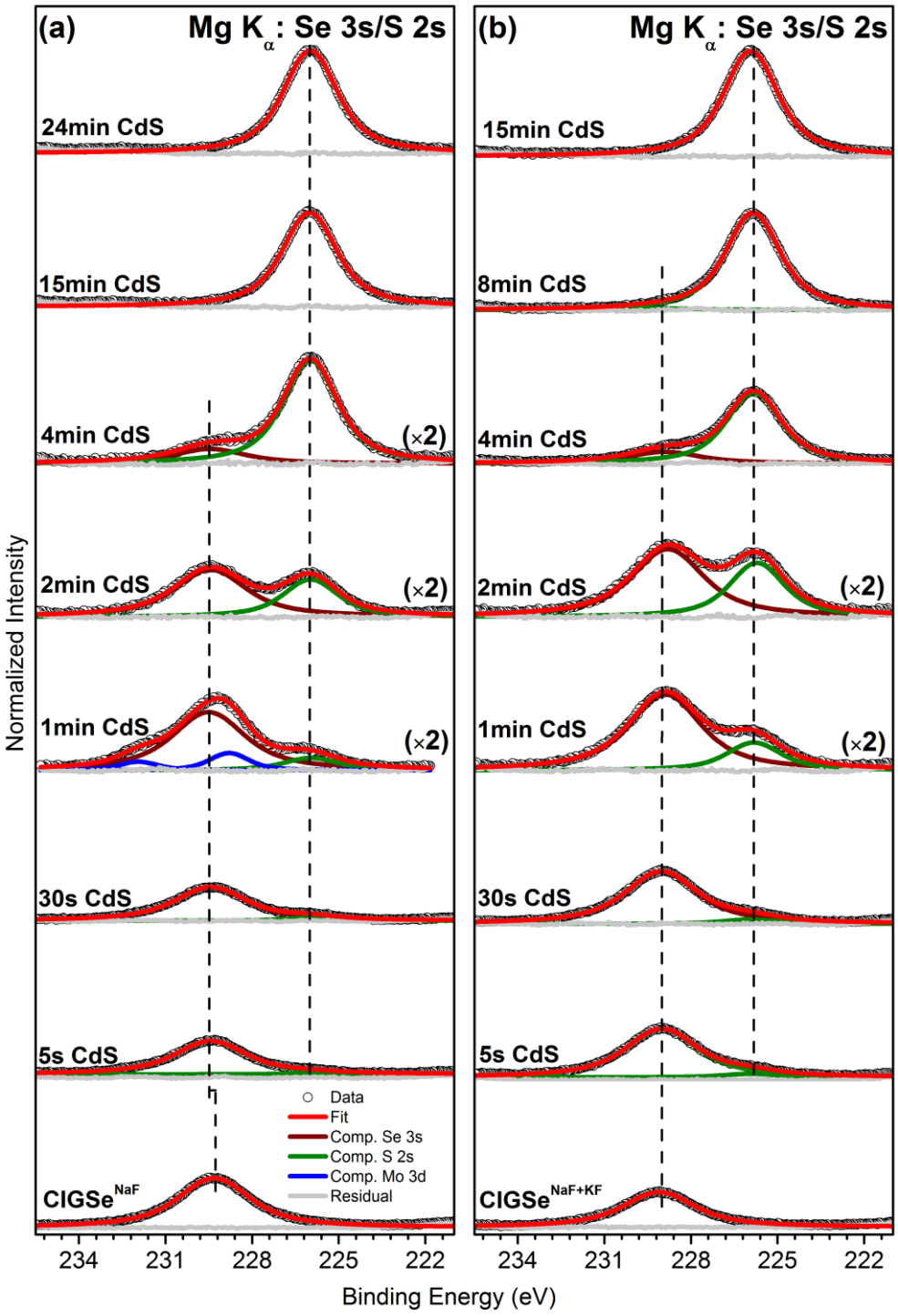

Figure S7. Se 3s/S 2s XPS data with respective Voigt fits of the CdS/CIGSe^{NaF} (a) and CdS/CIGSe^{NaF+KF} (b) sample series, measured with excitation energies of 1253.56 eV (Mg K_α). All spectra are displayed after subtraction of a linear background. For each fit, the residual is shown as well. Note the different magnification factors. Spectra are vertically offset for clarity.

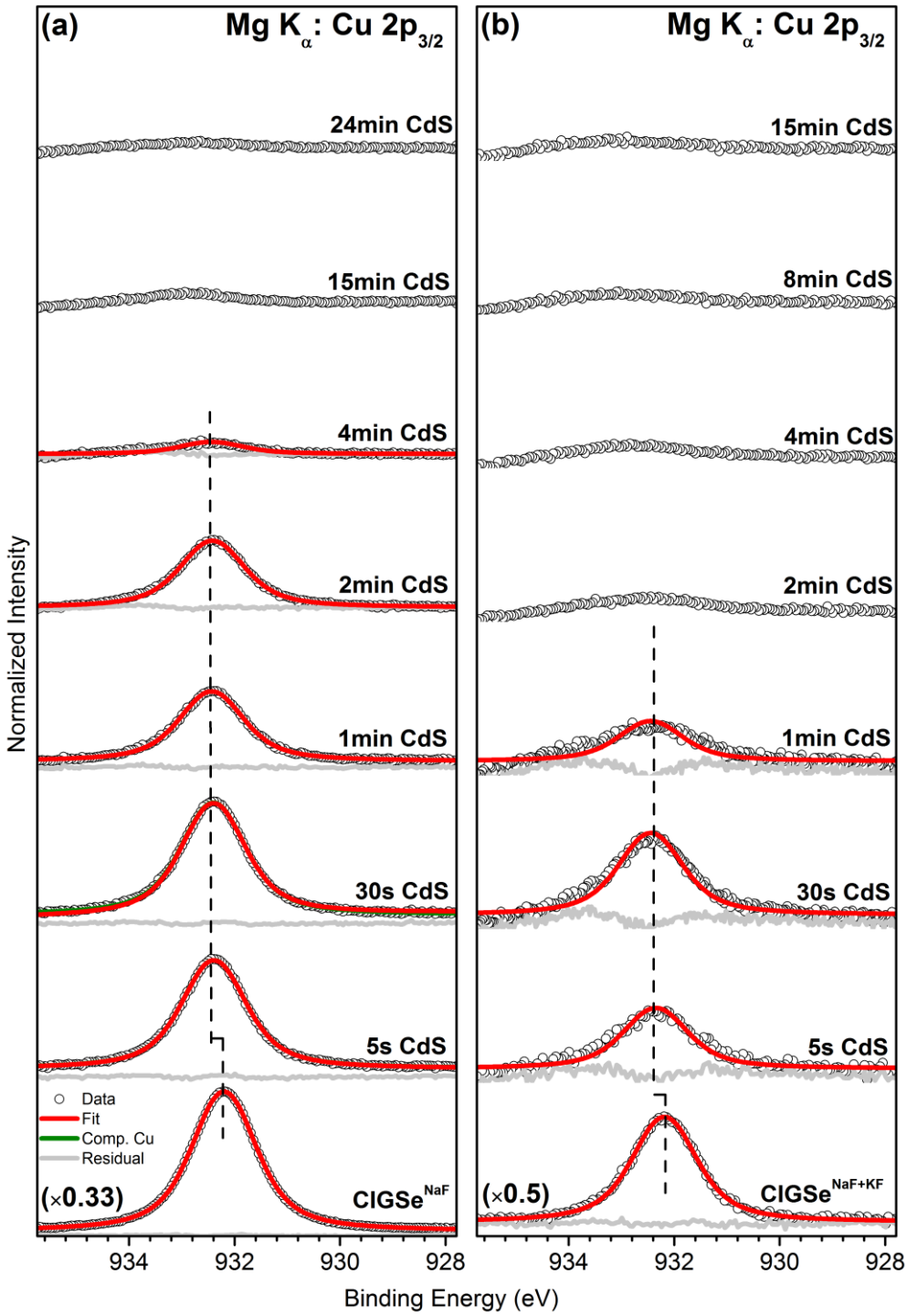

Figure S8. Cu $2p_{3/2}$ XPS data with respective Voigt fits of the CdS/CIGSe^{NaF} (a) and CdS/CIGSe^{NaF+KF} (b) sample series, measured with excitation energies of 1253.56 eV (Mg K_α). All spectra are displayed after subtraction of a linear background. For each fit, the residual is shown as well. Note the different magnification factors. Spectra are vertically offset for clarity.

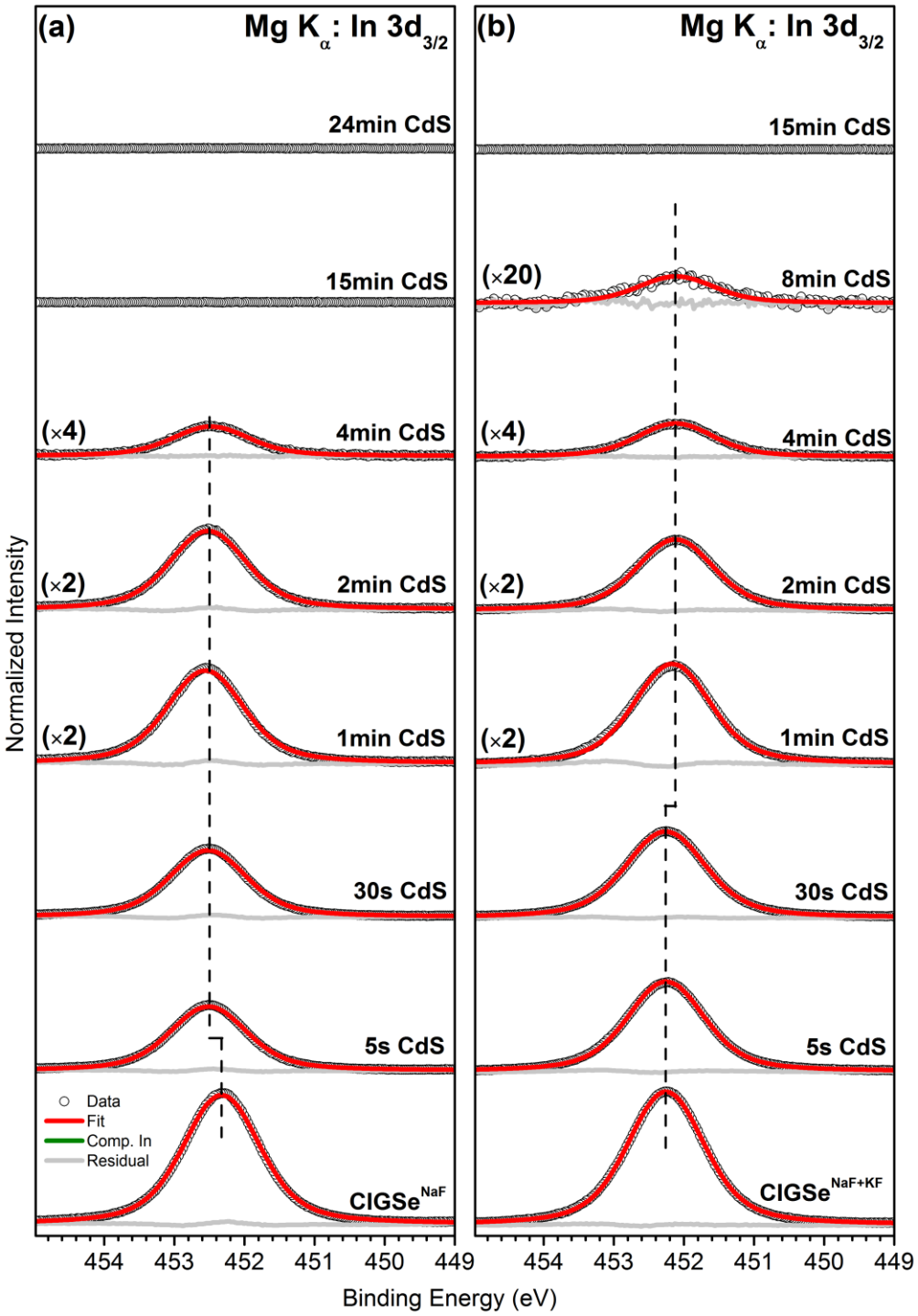

Figure S9. In $3d_{3/2}$ XPS data with respective Voigt fits of the CdS/CIGSe^{NaF} (a) and CdS/CIGSe^{NaF+KF} (b) sample series, measured with excitation energies of 1253.56 eV (Mg K_α). All spectra are displayed after subtraction of a linear background. For each fit, the residual is shown as well. Note the different magnification factors. Spectra are vertically offset for clarity.

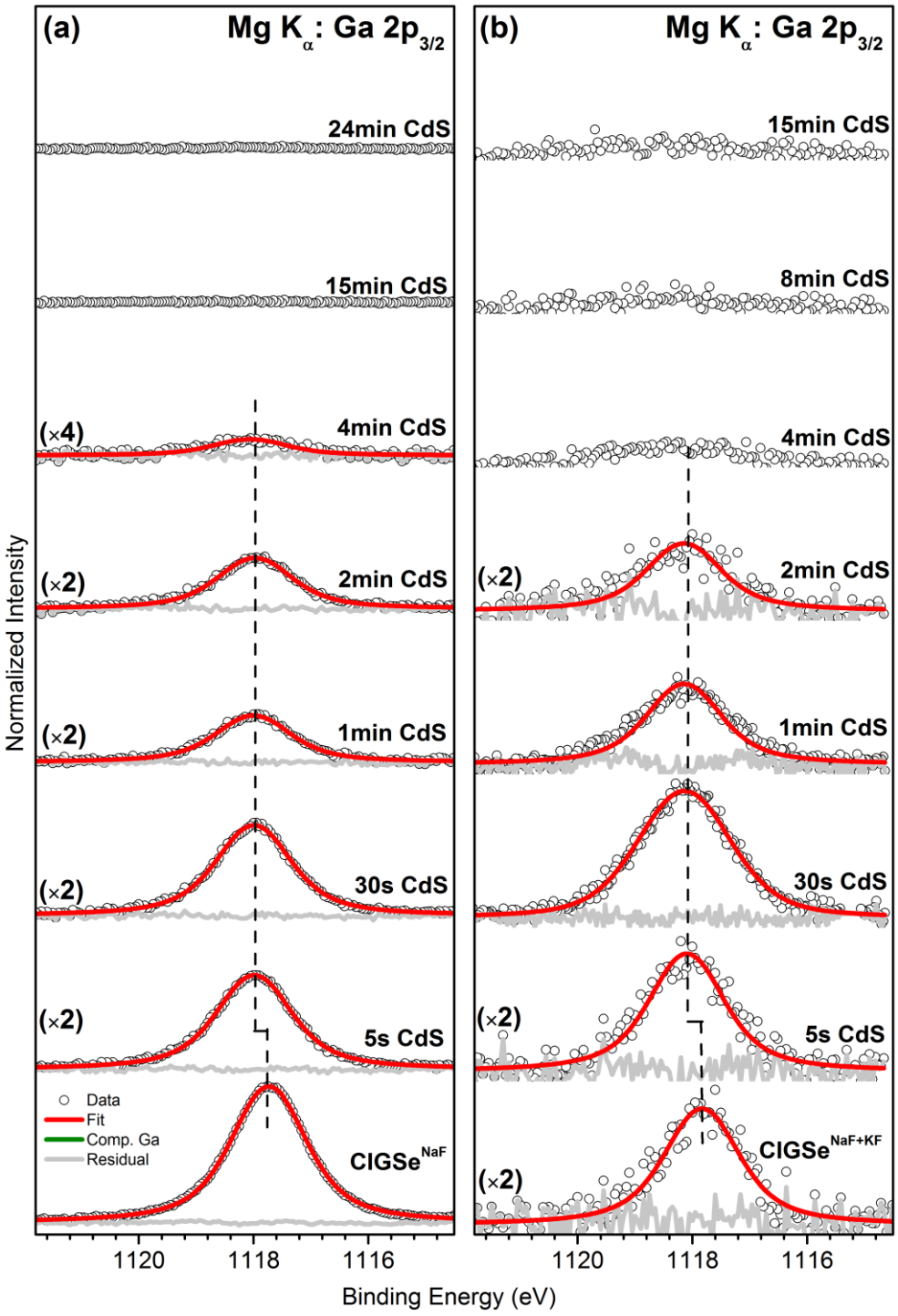

Figure S10. Ga $2p_{3/2}$ XPS data with respective Voigt fits of the CdS/CIGSe^{NaF} (a) and CdS/CIGSe^{NaF+KF} (b) sample series, measured with excitation energies of 1253.56 eV (Mg K_α). All spectra are displayed after subtraction of a linear background. For each fit, the residual is shown as well. Note the different magnification factors. Spectra are vertically offset for clarity.

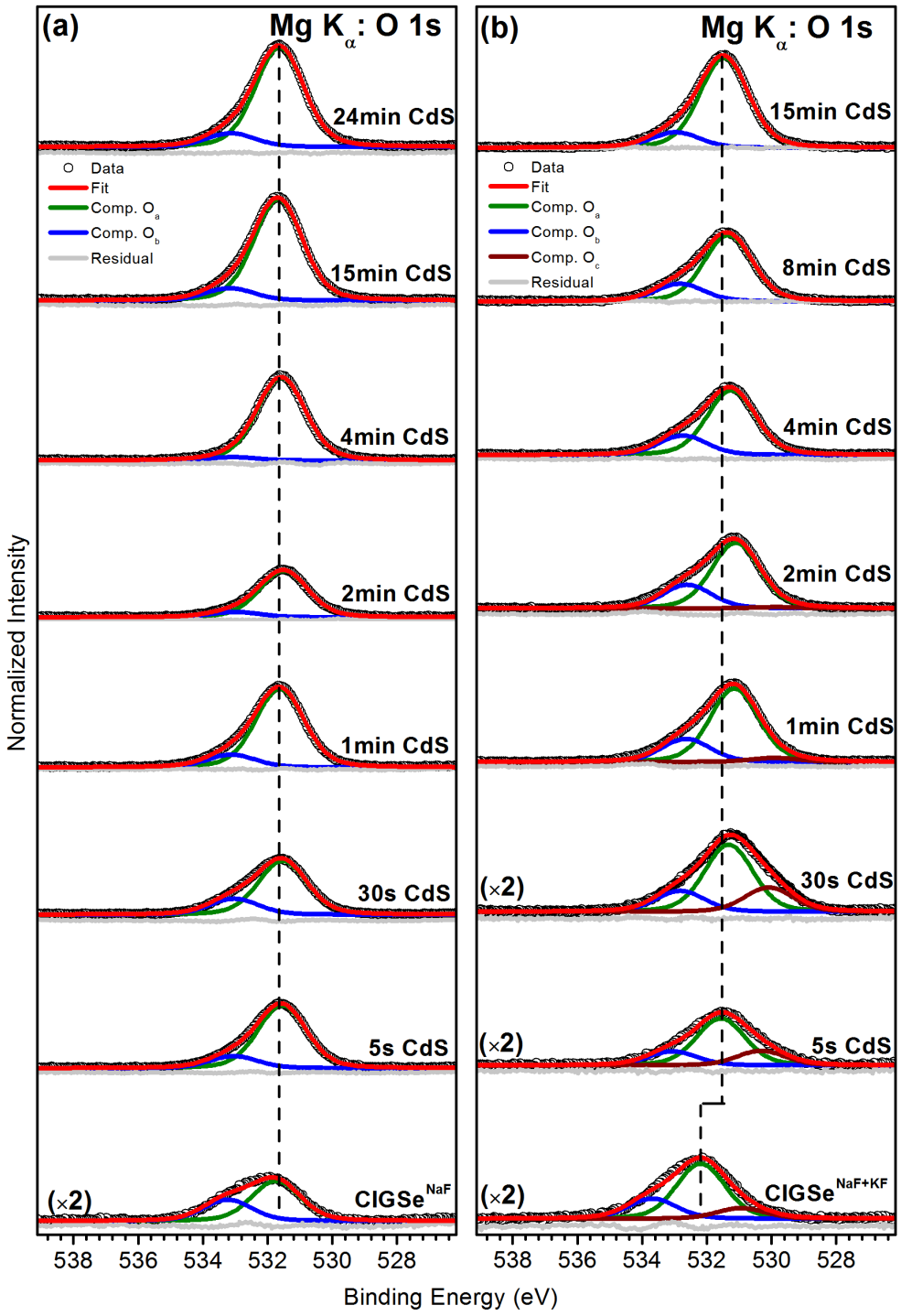

Figure S11. O 1s XPS data with respective Voigt fits of the CdS/CIGSe^{NaF} (a) and CdS/CIGSe^{NaF+KF} (b) sample series, measured with excitation energies of 1253.56 eV (Mg K$_\alpha$). All spectra are displayed after subtraction of a linear background. For each fit, the residual is shown as well. Note the different magnification factors. Spectra are vertically offset for clarity.

Figures S2-S11 show the detail spectra and corresponding fits of the background normalized Cu 3p, In 4d/Ga 3d, Se 3d, Na 1s (only for CdS/CIGSe^{NaF}), K 2p (only for CdS/CIGSe^{NaF+KF}), Cd 3d, Se 3s/S 2s, Cu 2p, In 3d, Ga 2p, and O 1s photoemission lines as a function of increasing

CBD time and for different PDT treatments. The Cu 3p spectra are shown after In 4p and Cd 4p background correction (see Figure S12-S15). As expected, most of absorber related signals decrease and the CdS buffer related signals increase in intensity with CBD time. All fits of a particular data set and for a particular photoemission line have been performed simultaneously using Voigt profiles with the same coupled Lorentz and Gauss widths. In case of spin-orbit doublet fits, the multiplicity rule (2j+1) is obeyed and the doublet separation for Cu 3p, In 4d, Ga 3d, Se 3d, and K 2p was set to 2.39 eV,[3] 0.86 eV,[4] 0.46 eV,[5] 0.83eV,[6] and 2.70 eV,[7] respectively. Note that the fit also included a linear background. Note that the Cd $3d_{3/2}$ and In $3d_{3/2}$ lines were chosen to fit instead of the more prominent respective $3d_{5/2}$ lines to avoid the Mg $K_{\alpha 3,4}$-excited $3d_{3/2}$ satellite lines that overlap with the $3d_{5/2}$ peak. All spectra but the O 1s line could be fit with one component. For O 1s more than one contribution (O_a and O_b for CdS/CIGSe^{NaF}; O_a, O_b, and O_c for CdS/CIGSe^{NaF+KF}) were needed for a satisfactory representation. Feature O_a at about 531.7 eV can be assigned to metal oxides [8-10], as e.g. In_2O_3,[8] Ga_2O_3,[9] or CdO.[10] Feature O_b located at 532.7 eV can be attributed to adsorbed hydroxyl species[11] and $Cd(OH)_2$[12]. The third component O_c between 530.0 and 530.8 eV which is only present in the data set of the CdS/CIGSe^{NaF+KF} series is attributed to potassium-oxygen bonds presumably with a mixed stoichiometry between K_2O and K_2O_2.[13] Note the small blue contribution to the Se 3s fit for the 1min CdS/CIGSe^{NaF} (Figure S7a) is attributed to a Mo 3d signal from the back contact presumably made accessible to the XPS analysis by accidental sample scratching during sample mounting. Furthermore, the broad signal detected at around 933 eV in Figure S8 for thicker CdS samples (i.e. ≥15 min for CdS/CIGSe^{NaF} and ≥2 min for CdS/CIGSe^{NaF+KF}) is ascribed to a Cd MNN plasmon background rather than to Cu $2p_{3/2}$.

All absorber layer related signals shift to lower binding energy for CdS/CIGSe^{NaF} sample series upon CdS deposition. The binding energy shift for CdS/CIGSe^{NaF+KF} series somewhat varies for every element, indicating a more complex situation.

3. Cu 3p background correction

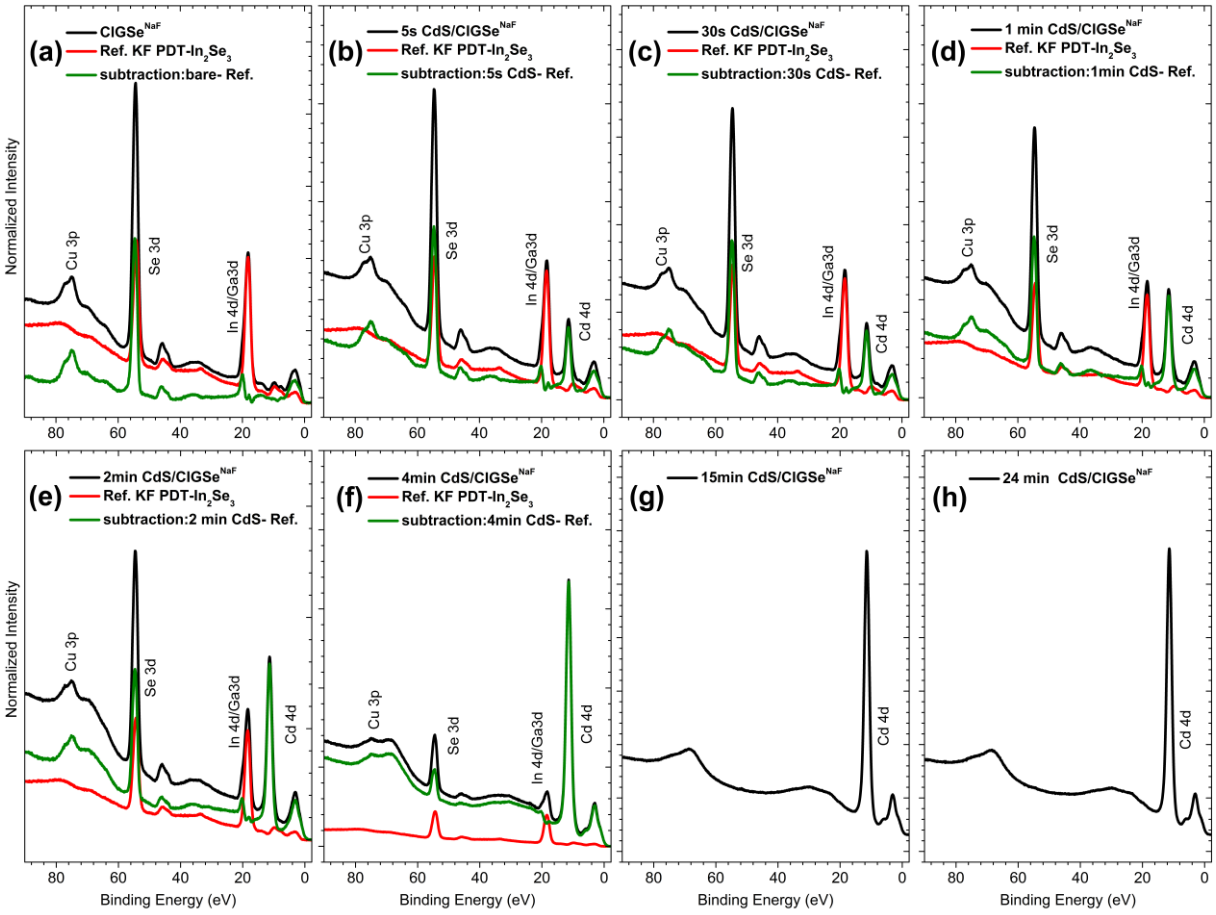

Figure S12. The In 4p background correction approach for the Cu 3p line using the respectively scaled and shifted In 4d line of the KF-PDT In_2Se_3 reference spectrum employed to the data set of the CdS/CIGSe^{NaF} sample series (CBD time: 0s (a), 5 s (b), 30 s, (c), 1 min (d), 2 min (e), 4 min (f) 15 min (g), and 24 min (h)), measured with an excitation energy of 1253.56 eV (Mg K_α). The as-measured spectra are shown in black, individually shifted and scaled references spectra in red, and the green spectra correspond to the resulting difference used for Cd 4p background.

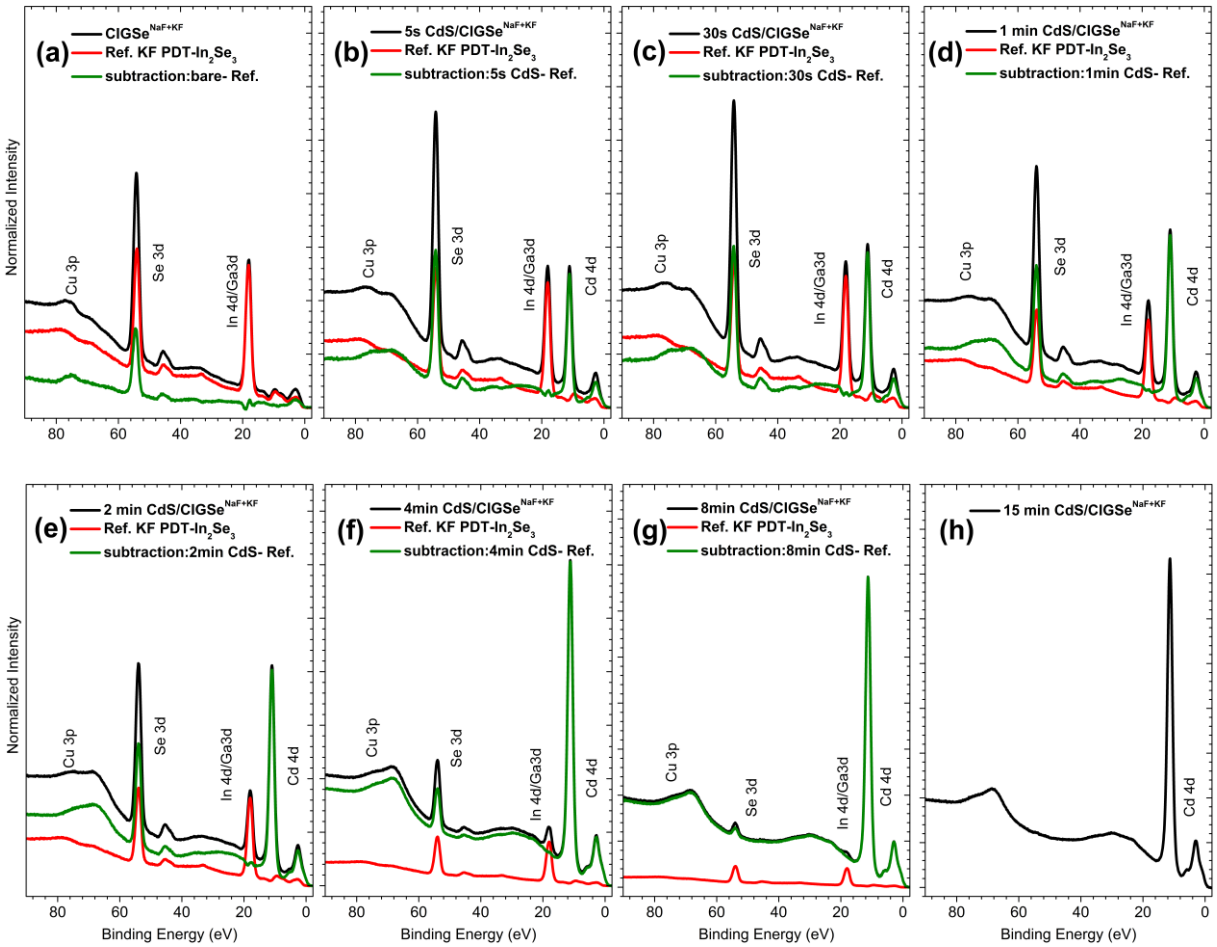

Figure S13. The In 4p background correction approach for the Cu 3p line using the respectively scaled and shifted In 4d line of the KF-PDT In_2Se_3 reference spectrum employed to the data set of the CdS/CIGSe^{NaF+KF} sample series (CBD time: 0s (a), 5 s (b), 30 s, (c), 1 min (d), 2 min (e), 4 min (f) 8 min (g), and 15 min (h)), measured with an excitation energy of 1253.56 eV (Mg K_α). The as-measured spectra are shown in black, individually shifted and scaled references spectra in red, and the green spectra correspond to the resulting difference used for Cd 4p background correction.

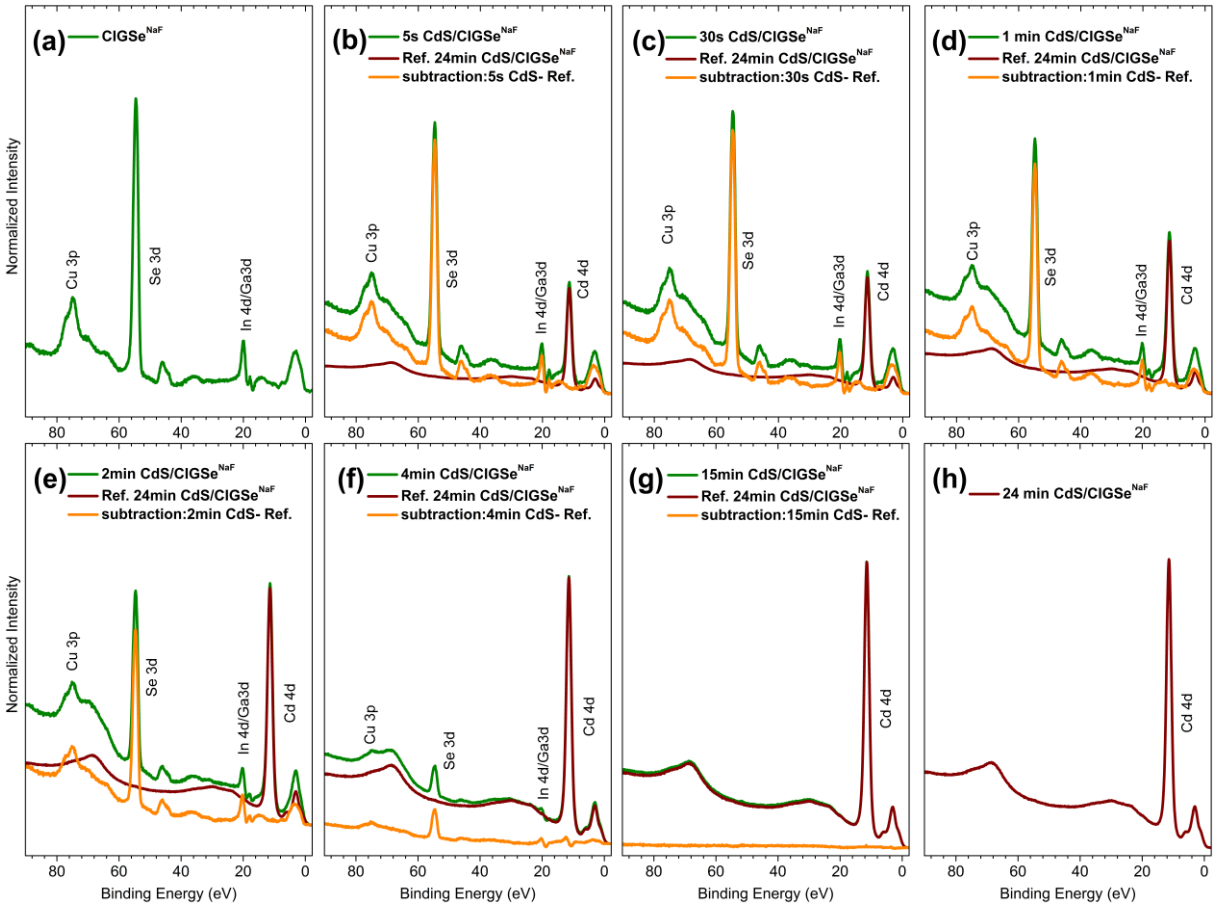

Figure S14. The Cd 4p background correction approach for the Cu 3p line using the respectively scaled and shifted Cd 4d line of the 24 min CdS/CIGSe^{NaF} sample employed to the whole data set (CBD time: 0s (a), 5 s (b), 30 s, (c), 1 min (d), 2 min (e), 4 min (f) 15 min (g), and 24 min (h)), measured with an excitation energy of 1253.56 eV (Mg K_α). The In 4p-corrected spectra are shown in green, individually shifted and scaled references spectra in wine, and the orange spectra correspond to the resulting difference used for further data evaluation.

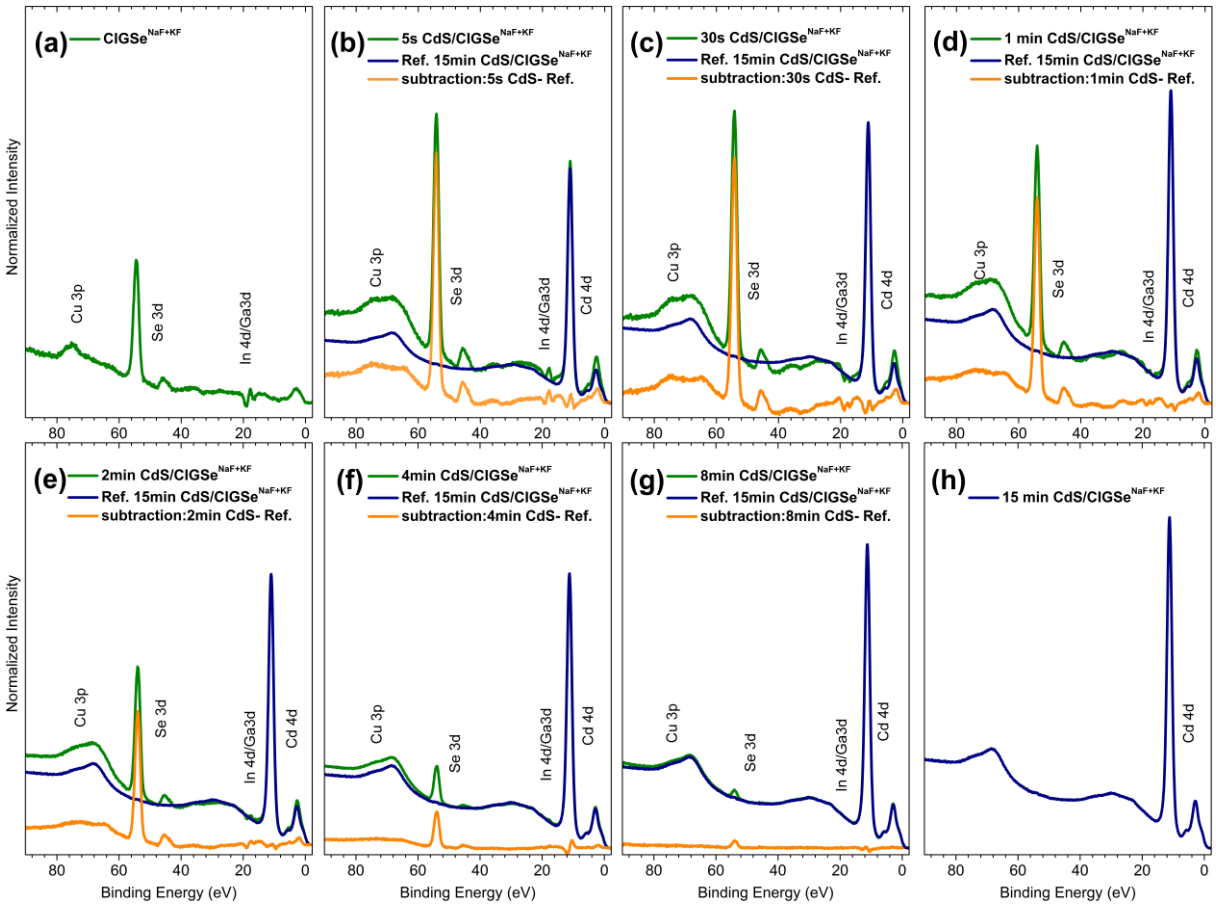

Figure S15. The Cd 4p background correction approach for the Cu 3p line using the respectively scaled and shifted Cd 4d line of the 15 min CdS/CIGSe^{NaF+KF} sample employed to the whole data set (CBD time: 0s (a), 5 s (b), 30 s, (c), 1 min (d), 2 min (e), 4 min (f) 8 min (g), and 15 min (h)), measured with an excitation energy of 1253.56 eV (Mg K_α). The In 4p-corrected spectra are shown in green, individually shifted and scaled references spectra in navy, and the orange spectra correspond to the resulting difference used for further data evaluation.

Figures S12-S15 visualize the Cu 3p background correction, subtracting (1) a properly shifted and scaled KF-PDT In_2Se_3 reference spectrum and (2) a properly shifted and scaled CdS reference spectrum (i.e., the spectrum of the thickest CdS sample of the respective sample series) to account for the broad In 4p and Cd 4p background (between 80 and 60 eV) that overlaps with the Cu 3p signal, respectively. For the proper energy shift and scaling factor for the reference spectra were derived by bringing the In 4d and Cd 4d lines, respectively, to maximum overlap. The "negative" overshoot in the range of the In 4d & Cd 4d line in the difference spectra can be explained by different composition profiles and/or slight variations of the core level binding energies.

4. Thickness calculation

The evolution of the intensity (mainly attenuation) of the absorber-related lines with CBD-CdS treatment periods is used to estimate the effective thickness of the attenuating buffer layers.

Based on the fitting results of the (shallow) core level spectra (Figures S2-S7), the buffer layer thickness is calculated based on the inelastic mean free path (IMFP) of the respective photoelectrons in CdS.[14] For absorber layer related elements, the intensity I^{abs} attenuated due to the increasing buffer layer and the effective buffer layer thickness d^{buf} are related – considering the used measurement geometry – according to the following formula:

$$I^{abs} = I_0 \times e^{-\frac{d^{buf}}{IMFP}} \quad (1)$$

where I_0 is the intensity of the lines of the bare CIGSe substrate. Note for this approach it is assumed that the buffer grows homogenously layer-by-layer.

Similarly, for buffer layer related elements, the effective buffer thickness d^{buf} and the intensity of the increasing buffer-related photoemission lines I^{buf} are related according to:

$$I^{buf} = I_1 \times (1 - e^{-\frac{d^{buf}}{IMFP}}) \quad (2)$$

Here I_1 is the intensity of the buffer-related photoemission lines for the thickest buffer layer (i.e., 24 min CdS/CIGS^{NaF} and 15 min CdS/CIGS^{NaF+KF}). The used IMFP values (in CdS) for the respective core level photoelectrons are shown in Table S1.

Table S1. Calculated inelastic mean free path for the different photoelectrons in CdS according to the TPP2M formula.[14]

Photoelectrons (excited with Mg K_α)	Inelastic mean free path [nm]
Cu 3p (E_K =1173.6 eV)	2.233
In 4d (E_K =1236.6 eV)	2.325
Ga 3d (E_K =1233.6eV)	2.321
Se 3d (E_K =1193.6 eV)	2.262
Cd 3d (E_K =838.6 eV)	1.738
S 2s (E_K =1023.6 eV)	2.008
Na 1s (E_K =178.6 eV)	0.642
K 2p (E_K =957.6 eV)	1.933

5. Se $M_{4,5}$: Area-normalized presentation & fit procedure

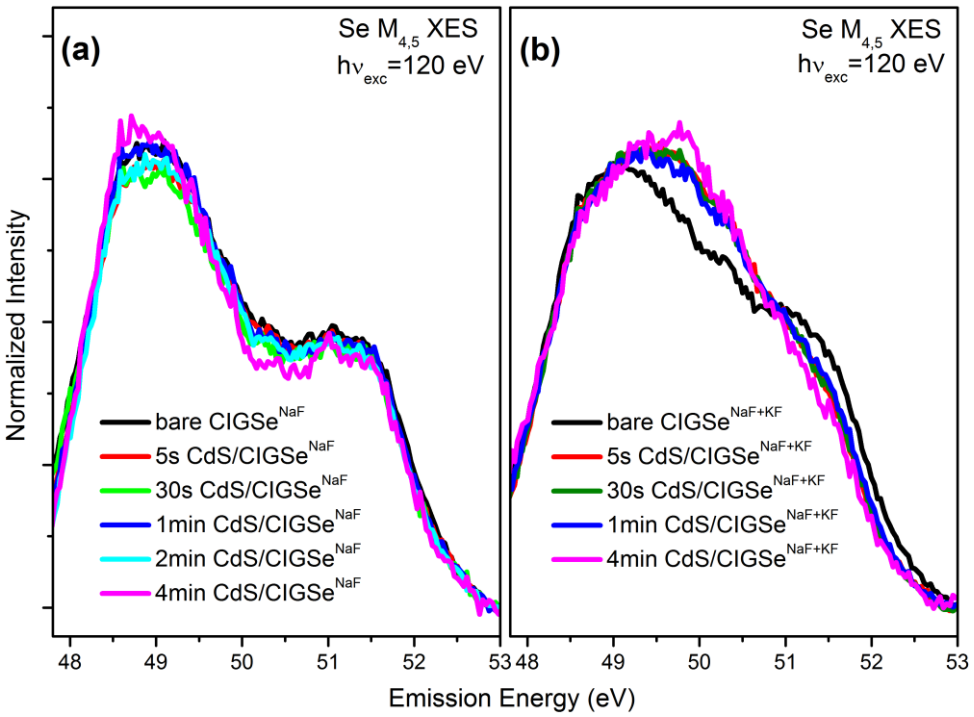

Figure S16. Area normalized Se $M_{4,5}$ XES spectra of the CdS/CIGSe^{NaF} (a) and CdS/CIGSe^{NaF+KF} (b) sample series.

The Se $M_{4,5}$ XES spectra of the CdS/CIGSe^{NaF+KF} sample set are represented by the sum of different reference spectra as shown in Figure S17 and S18. Figure S17 a and S18 a show the weighted sum of the spectrum of the CIGSe^{NaF} sample and that of the KF-PDT In_2Se_3 reference exactly representing the spectrum of the CIGSe^{NaF+KF} sample. This is an indication for the formation of a K-In-Se type species as a result of a NaF+KF PDT, corroborating previous results.[15] The representation of the spectra of the CdS/CIGSe^{NaF+KF} samples by the weighted sum of the spectrum of the bare CIGSe^{NaF} sample and that that of a CdSe reference is displayed in Figure S17 b-f. Figures S18 b-f show the representation of the same data set by the weighted sum of the spectrum of the bare CIGSe^{NaF+KF} sample and (again) that of a CdSe reference. The quantified values of the different spectral contributions are stated in the Figures, the uncertainty of these values is around ±0.03. The absolute area of the spectral residuals is also shown in the Figures above as a measure of the goodness of the fit. Apparently, the applied fit models (i.e., CIGSe^{NaF} + CdSe and CIGSe^{NaF+KF} + CdSe) result in similarly good fits.

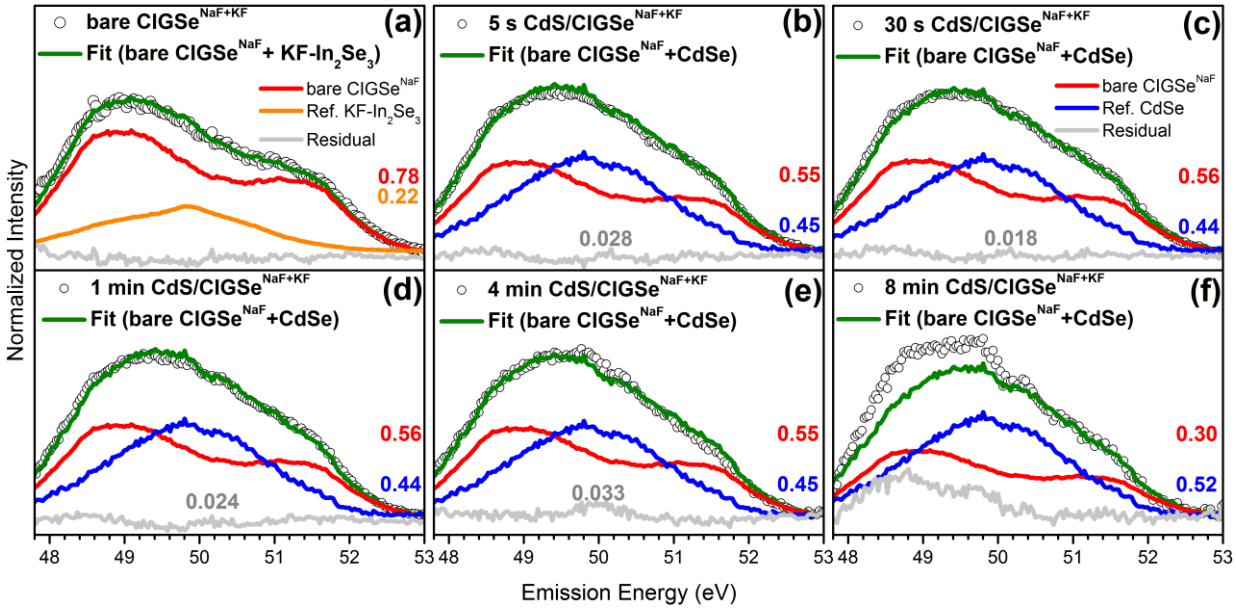

Figure S17. Se $M_{4,5}$ XES spectra of the CdS/CIGSe^{NaF+KF} sample set (CBD time: 0s (a), 5 s (b), 30 s, (c), 1 min (d), 4 min (e), and 8 min (f)) represented by a spectral sum (green) of the spectra of CIGSe^{NaF} (red), KF-PDT In_2Se_3 (orange) and CdSe (blue). The quantified values for the spectral contributions and the residuals are also shown. Furthermore, the absolute area of the spectral residuals is stated as measure for the goodness of the fit.

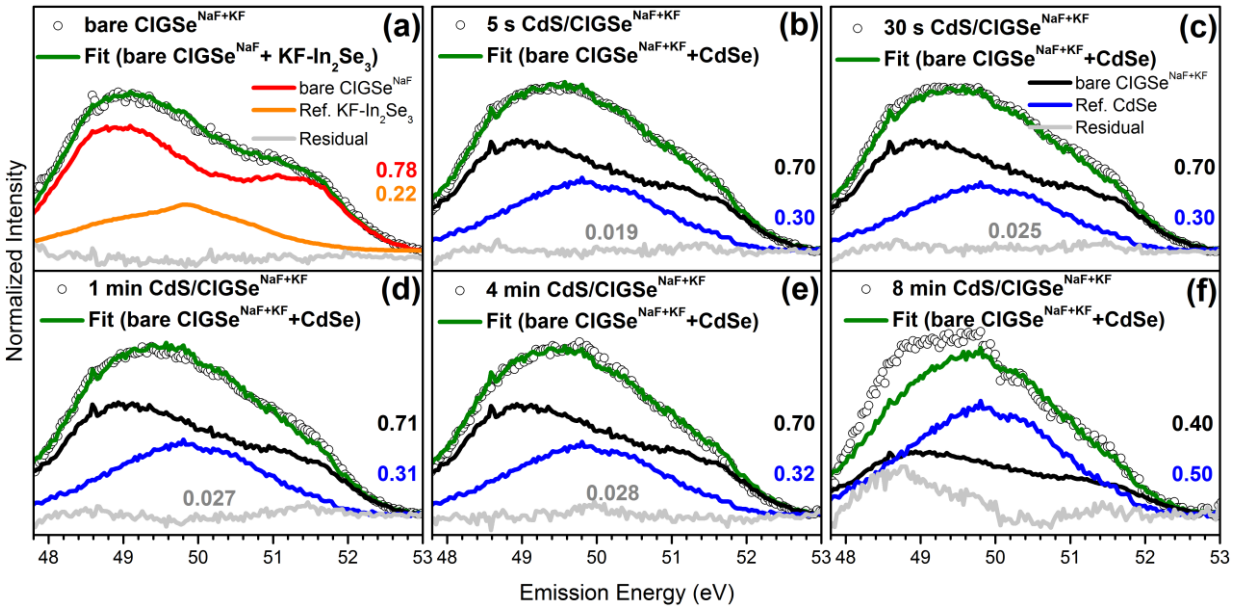

Figure S18. The Se $M_{4,5}$ XES spectrum of the CIGSe^{NaF+KF} sample (a) is represented by a spectral sum (green) of the spectra of CIGSe^{NaF} (red) and KF-PDT In_2Se_3 (orange) as shown in Figure S17a. The Se $M_{4,5}$ XES spectra of the CdS/CIGSe^{NaF+KF} sample set (CBD time: 5 s (b), 30 s, (c), 1 min (d), 4 min (e), and 8 min (f)) is represented by a spectral sum (green) of the spectra of CIGSe^{NaF+KF} (black) and CdSe (blue). The quantified values for the spectral contributions and the residuals are also shown. Furthermore, the absolute area of the spectral residuals is stated as measure for the goodness of the fit.

6. Comparison of K 2p and O 1s-related contributions

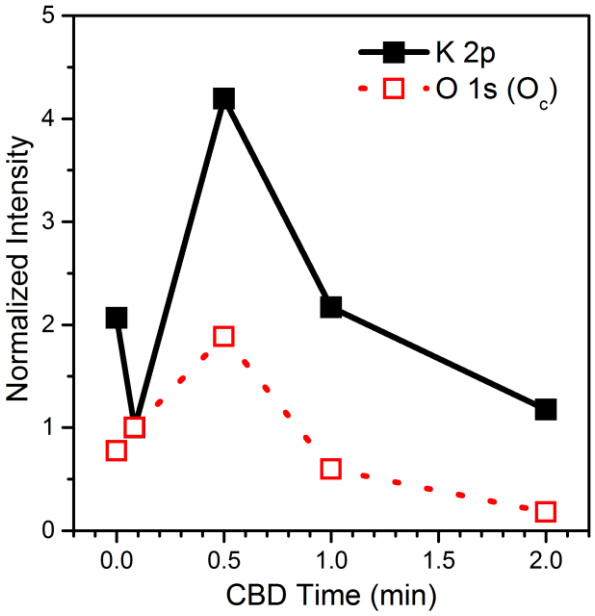

Figure S19. Intensity evolution of the K 2p (black) and O_c species (red) with increasing CBD time, normalized to the respective intensity values derived for the 5s CdS/CIGSe^{NaF+KF} sample.

As shown in Figure S11, there is a clear difference between the O 1s spectra of the CdS/CIGSe sample sets. In the CdS/CIGSe^{NaF+KF} series, an additional low-binding energy O 1s component (O_c) appears for CBD times ≤ 2 min. In the same CBD regime, we find a clear K 2p signal (Figure S5b) on the respective samples. Comparing the intensity evolution of the K $2p_{3/2}$ peak to that of the O 1s feature O_c in Figure S19, a clear correlation is revealed for CBD times ≥ 5s suggesting the presence of O-K bonds (see also discussion in conjunction to Figure S5b, above). The deviation for the bare absorber can be explained by potassium being present in a different chemical environment (→ K-In-Se type species). The significant intensity variation of the K 2p (and the O 1s (O_c)) line in the early stages of the CBD process indicates a complicated process involving dissolution and redeposition, or possibly diffusion. Furthermore, it should be considered that the formation of K-O bonds in this CBD time regime could very well be an artifact of sample preparation (i.e., retrieving the samples after the given time in the CBD solution with subsequent rinsing).

7. Cd MNN spectra: Background correction and fit

Since the Cd $M_{45}N_{45}N_{45}$ spectra (E_K: 370 eV~390eV) are significantly influenced by the In $M_{45}N_{45}N_{45}$ (E_K: 395 eV~415eV) spectra, In $M_{45}N_{45}N_{45}$ spectra were subtracted according to the fitting results depicted in Figure 3. The subtraction details are visualized in Figure S20.

After In $M_{45}N_{45}N_{45}$ background correction, peak-area-normalized Cd $M_4N_{45}N_{45}$ spectra were fitted, shown in Figure S21. Since Cd MNN Auger spectra of the thickest samples for each data set (i.e. the spectrum of the 24 min CdS/CIGSe^{NaF} sample and the spectrum of the 15 min CdS/CIGSe^{NaF+KF} sample) have the same spectral shape and are the narrowest, these spectra were also used as single-species references to (properly scaled and shifted) fit all other Cd MNN Auger spectra.

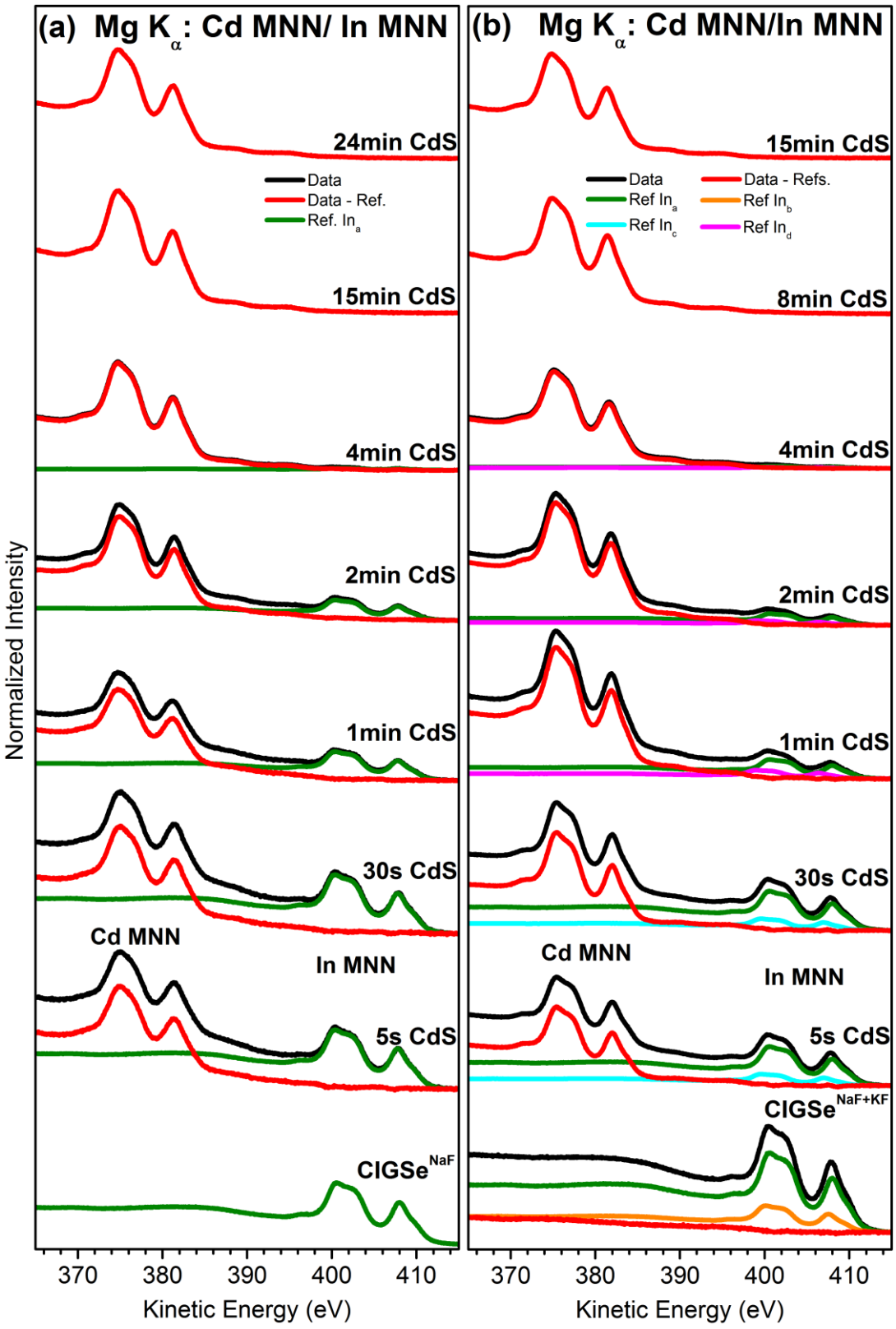

Figure S20. The In MNN background subtraction of the Cd MNN lines according to the fitting results in Figure 3 for the data set of the CdS/CIGSe^{NaF} (a) and CdS/CIGSe^{NaF+KF} (b) sample series, measured with an excitation energy of 1253.56 eV (Mg K$_\alpha$). The as-measured spectra are shown in black, individually shifted and scaled references spectra are depicted in green/orange/cyan/ magenta, and the red spectra represent to the background corrected Cd MNN Auger spectra. Spectra are vertically offset for clarity.

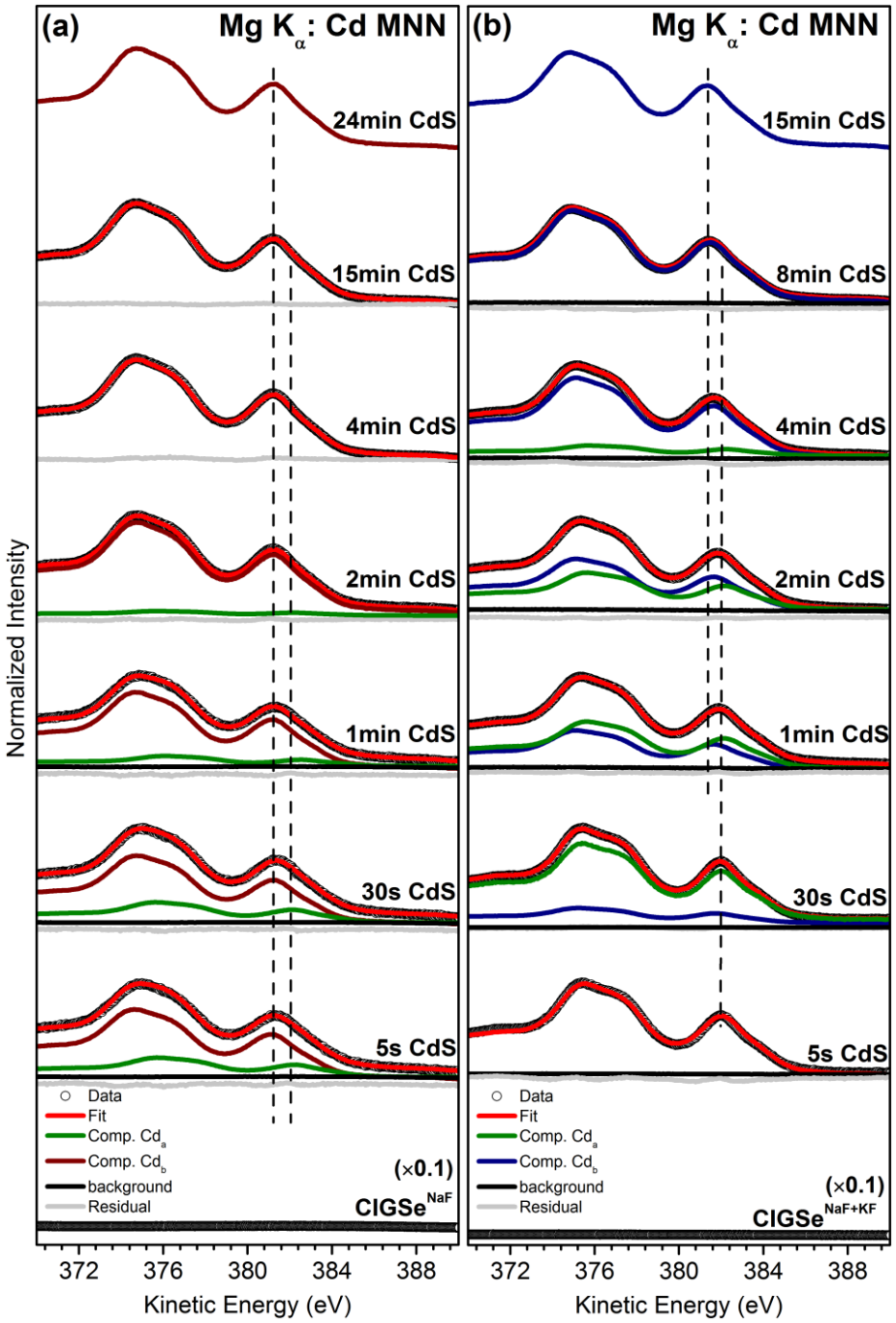

Figure S21. In MNN background-corrected Cd $M_{45}N_{45}N_{45}$ XAES lines of the CdS/CIGSe^{NaF} (a) and CdS/ PDT/CIGSe^{NaF+KF} (b) sample series with increasing CBD time, measured using Mg K_α excitation. Vertical offsets are added for clarity. The reference spectra representing component Cd_a or Cd_b are properly scaled and shifted Cd MNN spectra of the thickest sample per sample set (i.e., the spectrum of the 24 min CdS/CIGSe^{NaF} sample and that of the 15 min CdS/CIGSe^{NaF+KF} sample are used as single-species references).

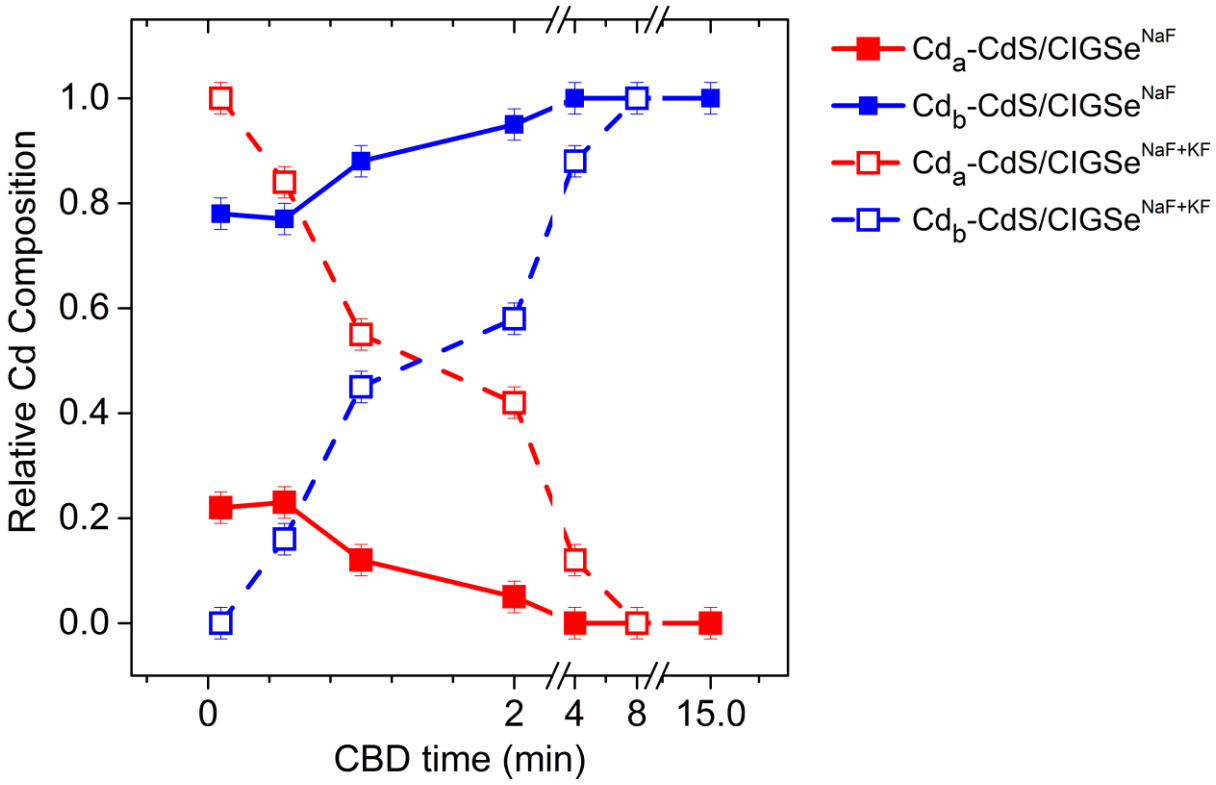

Figure S22. Relative Cd compound compositions of the CdS/CIGSe^{NaF} (solid square) and CdS/CIGSe^{NaF+KF} (open square) sample sets with increasing CBD time according to the Cd MNN fit results in Figure S21.

8. Definition of reference boxes for the comparison to derived modifed Auger parameters for In and Cd

In order to use the derived modified Auger parameters of In and Cd to identify different compounds, we ought to compare with reference values. However, there is only a very limited amount of modified Auger parameter values reported in literature. Thus, we constructed reference boxes that are based on the reported (very common) binding energy values for In 3d or Cd 3d and the reported kinetic energies of the corresponding MNN Auger line for a specific compound; when combined these values represent the largest possible spread of modified Auger parameters. In the following you will find a summary of the used binding and kinetic energy values used:

In previous reports, the In MNN Auger kinetic energies of In_2Se_3 are located between 408.0 - 408.3 eV.[16-17] Corresponding In $3d_{5/2}$ binding energies can be found between 444.3 and 445.1 eV.[16-18] Similarly, for $CuInSe_2$ we find 408.4 eV [18] and 443.9 eV[16] - 445 eV[19]; for $CuIn_3Se_5$ we find 407.4 eV [17] and 444.1 eV - 444.8 eV [16-17]; for In_2S_3 we find 407.3 - 407.4 eV [17, 20] and 444.7 - 445 eV[17, 20-21]; for In_2O_3 we find 406.0 - 406.8 eV [22-23] and 444.4 - 445 eV [18, 24]. Note that the doublet separation between In $3d_{3/2}$ (used in the analysis) and In $3d_{5/2}$ (for which reference values are reported) is 7.54 eV[25] and was considered when computing the modified Auger parameters derived from the measured data.

For the Cd modified Auger parameter, we followed a similar procedure. We combined the following kinetic energies of Cd MNN Auger and corresponding binding energies of Cd $3d_{5/2}$ peaks: for CdSe 381.20 eV – 381.90 eV [26-27] and 404.80 - 405.45 eV [17, 27-28]; for CdS 381.00 – 381.6 eV [17, 29] and 405.00 – 405.40 eV [30-31]; for $Cd(OH)_2$ 379.90 – 380.7 [29, 32] and 405.10 - 405.60 eV [32-34]; for CdO 382.1 - 382.7 eV [29, 34-35] and 404.00 – 405.2 eV.[17, 34-35]. Note that also in this case the doublet separation between Cd $3d_{5/2}$ and Cd $3d_{3/2}$ of 6.75 eV[36] has to be considered for the measured data.

9. The Cd/anion ratio of the deposited buffer layer

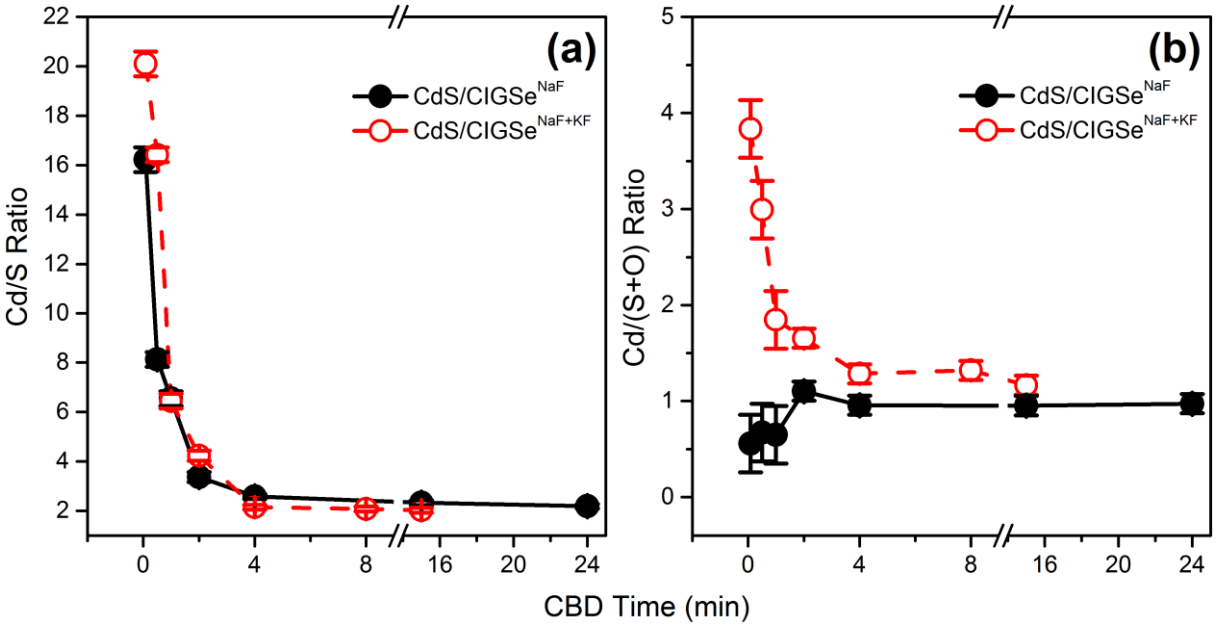

Figure S23. Evolution of (a) the Cd/S ratio and (b) the Cd/(S+O_{a+b}) ratio with increasing CBD time. The ratios were derived based on the fit results in Figures S6, S7, and S11, corrected by the respective inelastic mean free path (IMFP calculated by TPP2M[14]), analyzer transmission function, and photoionization cross section values.[37]

10. S $L_{2,3}$ XES: Direct comparison of CdS/CIGSe samples prepared in different temperature regimes

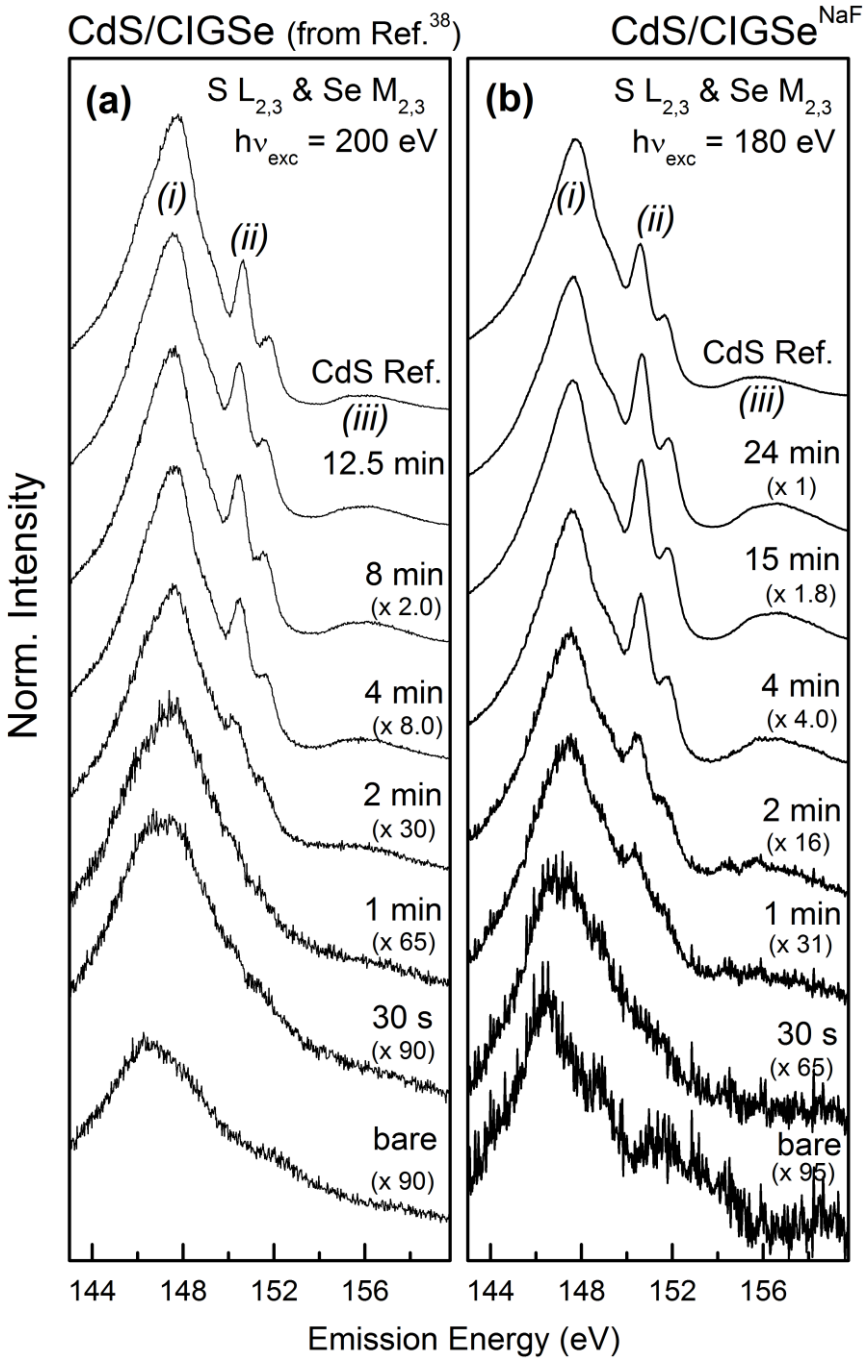

Figure S24. S $L_{2,3}$/Se $M_{2,3}$ XES spectra of K-free CdS/CIGSe samples as a function of CBD time prepared based on high-temperature processed ((a), Reproduced with permission from reference [38]. Copyright 2010 American Institute of Physics) and low-temperature processed ((b), compare to Figure 6a of this study) CIGSe absorber. The main features are labeled (i)−(iii). Spectra are normalized to equal peak height above background and vertically offset for clarity. Note the different magnification factors.

In order to compare the findings related to the chemical structure of the (buried) CdS/CIGSe^{NaF} with reports in literature, Figure S24 shows a direct comparison of the S $L_{2,3}$/Se $M_{2,3}$ XES

spectra to previously measured XES data of a similar CdS/CIGSe sample set (from Ref.[38]). The main difference in the sample sets is the fact that the absorbers of the different series were prepared in different temperature regimes. While the absorbers of this study have been prepared at low temperatures (to facilitate the employment of flexible polyimide type substrates), the absorber used in the previous study was deposited at higher temperatures. In addition, for the low temperature processed CIGSe absorber of the current study a PDT was performed, while for the high temperature processed absorbers of the previous study one relied on the diffusion from the soda-lime glass as the sole sodium source. Nevertheless, at first sight, the spectra look very similar. The main features are associated with[39] (i) S 3s states, (ii) Cd 4d-derived bands (i.e., Cd 4d → S $2p_{3/2}$, and Cd 4d → S $2p_{1/2}$ transitions, respectively), and (iii) the upper valence band (UVB). However close inspection of the spectra, in particular those that represent samples with buffer layers that have been deposited within short (i.e., 1 and 2 min) CBD times, reveals that the Cd 4d-derived features are differently pronounced. In the old data sat, the Cd 4d-derived features are (almost) completely missing (for the 1 min CdS/CIGSe sample) and significantly reduced in intensity (for the 2 min CdS/CIGSe sample) compared to the spectra of the respective CdS/CIGSe^{NaF} samples of this study. Previously, the apparent presence of S-related spectral intensity without the presence of the Cd 4d-derived features was interpreted as a CBD-CdS process induced S-deposition without the deposition of Cd / the formation of S-Cd bonds. In this particular case, it was concluded that an $(In_{1-x}Ga_x)_ySz$ type interface layers between CdS and the CIGSe absorber is formed.[38]

In the current case, we can clearly identify Cd 4d-derived features in the spectrum of the 1 min CdS/CIGSe^{NaF} sample, which indicates a significantly reduced induction period of the CBD-CdS process may be caused by a different surface structure of the low temperature processed and PDTed CIGSe absorber.

References

(1) Hüfner, S. *Photoelectron Spectroscopy: Principles and Applications*, Springer: 2013.

(2) Bär, M.; Weinhardt, L.; Heske, C. Soft X‐ray and Electron Spectroscopy: A Unique "Tool Chest" to Characterize the Chemical and Electronic Properties of Surfaces and Interfaces. In *Advanced Characterization Techniques for Thin Film Solar Cells*; Abou‐Ras, D. K., T.; Rau. U., Ed.; Wiley-VCH: Weinmheim, Germany, 2016.

(3) Lebugle, A.; Axelsson, U.; Nyholm, R.; Martensson, N. Experimental L and M Core Level Binding Energies for the Metals ^{22}Ti to ^{30}Zn. *Phys. Scr.* **1981,** *23*, 825-827.

(4) Poole, R. T.; Kemeny, P. C.; Liesegang, J.; Jenkin, J. G.; Leckey, R. C. G. High Resolution Photoelectron Studies of the d Bands of Some Metals. *J. Phys. F: Metal Phys.* **1973,** *3*, L46-L48.

(5) Poirier, D. M.; Weaver, J. H. GaAs(110) by XPS. *Surface Science Spectra* **1993,** *2*, 201-208.

(6) Shevchik, N. J.; Cardona, M.; Tejeda, J. X-Ray and Far-uv Photoemission from Amorphous and Crystalline of Se and Te. *Phys. Rev. B* **1973,** *8*, 2833-2841.

(7) Petersson, L. G.; Karlsson, S. E. Clean and Oxygen Exposed Potassium Studied by Photoelectron Spectroscopy. *Phys. Scr.* **1977,** *16*, 425-431.

(8) Sutter, E. A.; Tong, X.; Jungjohann, K.; Sutter, P. W. Oxidation of Nanoscale Au–In Alloy Particles as A Possible Route Toward Stable Au-Based Catalysts. *PNAS* **2013,** *110*, 10519.

(9) Shalish, I.; Shapira, Y.; Burstein, L.; Salzman, J. Surface States and Surface Oxide in GaN Layers. *J. Appl. Phys.* **2001,** *89*, 390-394.

(10) Eom, N. S. A.; Kim, T. S.; Choa, Y. H.; Kim, W. B.; Kim, B. S. Surface Oxidation Behaviors of Cd-Rich CdSe Quantum Dot Phosphors at High Temperature. *J. Nanosci. Nanotechnol.* **2014,** *14*, 8024-8027.

(11) Brown, M. A.; Fujimori, Y.; Ringleb, F.; Shao, X.; Stavale, F.; Nilius, N.; Sterrer, M.; Freund, H.-J. Oxidation of Au by Surface OH: Nucleation and Electronic Structure of Gold on Hydroxylated MgO(001). *J. Am. Chem. Soc.* **2011,** *133*, 10668-10676.

(12) Kishi, K.; Ikeda, S. X-Ray Photoelectron Spectroscopic Study for the Reaction of Evaporated Iron with O_2 and H_2O. *Bull. Chem. Soc. Jpn.* **1973,** *46*, 341-345.

(13) Kim, M. G.; Kanatzidis, M. G.; Facchetti, A.; Marks, T. J. Low-Temperature Fabrication of High-Performance Metal Oxide Thin-Film Electronics via Combustion Processing. *Nat. Mater.* **2011,** *10*, 382-388.

(14) Tanuma, S.; Powell, C. J.; Penn, D. R. Calculations of Electron Inelastic Mean Free Paths. *Surf. Interface Anal.* **1993,** *20*, 77-89.

(15) Handick, E.; Reinhard, P.; Wilks, R. G.; Pianezzi, F.; Kunze, T.; Lorenzo, D. K.; Weinhardt, L.; Blum, M.; Yang, W.; Gorgoi, M.; Ikenaga, E.; Gerlach, D.; Ueda, S.; Yamashita, Y.;Chikyow, T.; Heske, C.; Buecheler, S.; Tiwari, A. N.; Bär, M. Formation of a K-In-Se Surface Species by NaF/KF PostdepositionTreatment of Cu(In,Ga)Se_2 Thin-Film Solar Cell Absorbers. *ACS Appl. Mater. Interfaces* **2017,** *9*, 3581-3589.

(16) Cahen, D.; Ireland, P. J.; Kazmerski, L. L.; Thiele, F. A. X-ray Photoelectron and Auger Electron Spectroscopic Analysis of Surface Treatments and Electrochemical Decomposition of $CuInSe_2$ Photoelectrodes. *J. Appl. Phys.* **1985,** *57* (10), 4761-4771.

(17) Moulder, J. F.; Stickle, W. F.; Sobol, P. E.; Bomben, K. D. *Handbook of X-Ray Photoelectron Spectroscopy*, Minnesota, USA, 1995.

(18) Kazmerski L. L.; Jamjoum O.; Ireland P. J.; Deb, S. K. R.; Mickelsen A.; Chen W. Initial Oxidation of $CuInSe_2$. *J. Vacuum Sci. & Technol.* **1981,** *19*, 467-471.

(19) Von Morzé, N.; Dittrich, T.; Calvet, W.; Lauermann, I.; Rusu M. Transient and Modulated Charge Separation at $CuInSe_2$/C60 and $CuInSe_2$/ZnPc Hybrid Interfaces. *Appl. Surf. Sci.* **2017,** *396*, 366-374.
(20) Sterner, J.; Malmström, J.; Stolt, L. Study on ALD In_2S_3/Cu(In,Ga)Se_2 Interface Formation. *Prog. Photovolt. Res. Appl.* **2005,** *13*, 179-193.
(21) Briggs, D.; Seah, M. P. *Practical Surface Analysis: Auger and X-ray Photoelectron Spectroscopy*, Wiley: New York 1983.
(22) Faur, M.; Jayne, D. T.; Goradia, M.; Goradia, C. XPS Investigation of Anodic Oxides Grown on P-type InP. *Surf. Interface Anal.* **1990,** *15*, 641-650.
(23) Lin, A. W. C.; Armstrong N. R.; Kuwana, T. X-ray Photoelectron/Auger Electron Spectroscopic Studies of Tin and Indium Metal Foils and Oxides. *Ana. Chem.* **1977,** *49*, 1228-1235.
(24) Bertrand, P. A. XPS Study of Chemically Etched GaAs and InP. *J. Vacuum Sci. & Technol.* **1981,** *18*, 28-33.
(25) Dai, M. Z.; Khan, K.; Zhang, S. N.; Jiang, K. J.; Zhang, X. Y.; Wang, W. L.; Liang, L. Y.; Cao, H. T.; Wang, P. J.; Wang, P.; Miao, L. J.; Qin, H. M.; Jiang, J.; Xue, L. X.; Chu, J. H. A Direct Method to Extract Transient Sub-Gap Density of State (DOS) Based on Dual Gate Pulse Spectroscopy. *Sci. Rep.* **2016,** *6*, 24096.
(26) Islam, R.; Rao, D. R. X-ray Photoelectron Spectroscopy of $Zn_{1-x}Cd_xSe$ Thin Films. *J. Electron. Spectrosc. Relat. Phenom.* **1996,** *81*, 69-77.
(27) Polak, M. X-Ray Photoelectron Spectroscopic Studies of $CdSe_{0.65}Te_{0.35}$. *J. Electron. Spectrosc. Relat. Phenom.* **1982,** *28*, 171-176.
(28) Banerjeea, S.; Wong, S. S. Formation of CdSe Nanocrystals onto Oxidized, Ozonized Single-Walled Carbon Nanotube Surfaces. *ChemComm* **2004**, 1866-1867.
(29) Niles, D. W.; Herdt, G.; Al-Jassim, M. An X-ray Photoelectron Spectroscopy Investigation of O Impurity Chemistry in CdS Thin Films Grown by Chemical Bath Deposition. *J. Appl. Phys.* **1997,** *81*, 1978-1984.
(30) Bhide, V. G.; Salkalachen, S.; Rastog, A. C.; Rao, C. N. R.; Hegde, M. S. Depth Profile Composition Studies of Thin Film CdS:Cu_2S Solar Cells Using XPS and AES. *J. Phys. D: Appl. Phys.* **1981,** *14*, 1647-1656.
(31) Riga, J.; Verbist, J. J.; Josseaux, P.; Mesmaeker, A. K. Correlation between CdS Photoanodic Behaviour and Electrode Chemical Modifications: An X‐ray Photoelectron Spectroscopic Study. *Surf. Interface Anal.* **1985,** *7*, 163-168.
(32) Wagner C.D.; Gale L. H.; Raymond, R. H. Two-Dimensional Chemical State Plots: A Standardized Data Set for Use in Identifying Chemical States by X-ray Photoelectron Spectroscopy. *Ana. Chem.* **1979,** *51*, 466-482.
(33) Zhang, D. E.; Pan, X. D.; Zhu, H.; Li, S. Z.; Xu, G. Y.; Zhang, X. B.; Ying, A. L.; Tong, Z. W. A Simple Method to Synthesize Cadmium Hydroxide Nanobelts. *Nanoscale Res. Lett.* **2008,** *3* (8), 284-288.
(34) Tkachenko, O. P.; Shpiro, E. S.; Wark, M.; Ekloff, G. S.; Jaeger, N. X-Ray Photoelectron/X-Ray Excited Auger Electron Spectroscopic Study of Highly Dispersed Semiconductor CdS and CdO Species in Zeolites. *J. Chem. Soc. Faraday Trans.* **1993,** *89*, 3987-3994.
(35) Gaarenstroom, S. W.; Winograd, N. Initial and Final State Effects in the ESCA Spectra of Cadmium and Silver Oxides. *J. Chem. Phys.* **1977,** *67*, 3500-3506.
(36) White, H. S.; Rlcco, A. J.; Wrighton, M. S. Characterization of p-Type CdTe Electrodes in Acetonitrile/Electrolyte Solutions. Nearly Ideal Behavior from Reductive Surface Pretreatments. *J. Phys. Chem. C* **1983,** *87*, 5140-5150.

(37) Trzhaskovskaya, M. B. Photoelectron Angular Distribution Parameters for Elements Z= 1 to Z=54 in the Photoelectron Energy Range 100-5000eV. *At. Data Nucl. Data Tables* **2001,** *77*, 97-159.
(38) Pookpanratana, S.; Repins, I.; Bär, M.; Weinhardt, L.; Zhang, Y.; Félix, R.; Blum, M.; Yang, W.; Heske C. CdS/Cu(In,Ga)Se_2 Interface Formation in High-Efficiency Thin Film Solar Cells. *Appl. Phys. Lett.* **2010,** *97*, 074101.
(39) Bär, M.; Repins, I.; Weinhardt, L.; Alsmeier, J.-H.; Pookpanratana, S.; Blum, M.; Yang, W.; Heske, C.; Wilks, R. G.; Nouf, R. Zn−Se−Cd−S Interlayer Formation at the CdS/$Cu_2ZnSnSe_4$ Thin-Film Solar Cell Interface. *ACS Energy Lett.* **2017,** *2*, 1632-1640.